Scanning Microscopy

Volume 1995
Number 9 *Luminescence*

Article 3

1995

Cathodoluminescence of Rare Earth Doped Zircons. I. Their Possible Use as Reference Materials

F. Cesbron
ESEM, Orléans, France

P. Blanc
Université P. et M. Curie, Paris

D. Ohnenstetter
Vandoeuvre-les-Nancy, France

G. Rémond
BRGM, Orléans, France, guy@valcofim.fr

Scanning Microscopy Supplement 9, 1995 (Pages 35-56) 0892-953X/95$5.00+.25
Scanning Microscopy International, Chicago (AMF O'Hare), IL 60666 USA

CATHODOLUMINESCENCE OF RARE EARTH DOPED ZIRCONS. I. THEIR POSSIBLE USE AS REFERENCE MATERIALS

F. Cesbron[1], P. Blanc[2], D. Ohnenstetter[3], G. Rémond[4,*]

[1]URA-CNRS 1366, ESEM, Orléans, France; [2]URA-CNRS 1761, Université P. et M. Curie, Paris, France; [3]CRPG, CNRS, Vandoeuvre-les-Nancy, France; [4]BRGM, Orléans, France

Abstract

Synthetic zircon crystals ($ZrSiO_4$), undoped and doped with Y^{3+}, La^{3+}, Ce^{3+}, Pr^{3+}, Nd^{3+}, Sm^{3+}, Eu^{3+}, Gd^{3+}, Tb^{3+}, Dy^{3+}, Ho^{3+}, Er^{3+}, Tm^{3+}, Yb^{3+}, Lu^{3+}, were grown from a flux consisting of a mixture of Li_2MoO_4 and MoO_3 heated to 1125°C and then cooled to 750°C. The cathodoluminescence (CL) spectra of these zircons were analyzed at room-temperature and near liquid nitrogen temperature with a CL spectrometer attached to a scanning electron microscope (SEM). This study highlights the complexity of the intrinsic emission band extending from 200 to 500 nm. The relative intensities of the major emission band centered at 230 nm (5.4 eV) and peaks of less energy were found to depend upon the crystallographic orientation of the crystals. Sm^{3+}, Eu^{3+}, Gd^{3+}, Tb^{3+}, Dy^{3+}, Ho^{3+}, Er^{3+} and Tm^{3+}-doped zircons display sharp emission peaks being characteristic of the doping rare-earth element (REE). These lines are frequently multiplets but only the average position of the peaks are reported because of the instrumental conditions used in this study. The CL intensities of the intrinsic and extrinsic features were found to depend on the crystal orientation, and numerous experimental factors such as the electron beam energy and the beam current density.

Key Words: Zircon, undoped synthetic zircon, REE-doped synthetic zircon, cathodoluminescence, cathodoluminescence anisotropy, intrinsic luminescent centers, REE luminescent ions.

*Address for correspondence and present address:
G. Rémond
32 Avenue de la Mouillere,
45100 Orléans, France
Telephone number: 33-38-66 66 62
E.mail: guy@valcofim.fr

Introduction

Emission of cathodoluminescence (CL), observed using an electron probe microanalyzer (EPMA) or a scanning electron microscope (SEM), has been used as a petrologic tool since Long and Agrell (1965), Smith and Stenstrom (1965) and Coy-Yll (1969/70). The CL images of minerals can be compared with secondary or backscattered electron images (BSE) and X-ray mapping (Rémond *et al.*, 1970, 1992; Rémond, 1977). Such image comparisons were recently published for zircon crystals (Henry and Toney, 1987; Hanchar and Miller, 1993).

Cathodoluminescence microscopy has been shown to provide a rapid method for revealing the spatial distribution of defects in minerals, some of which being associated with the presence of trace elements. However, CL spectroscopy, as a general analytical tool for the identification of impurities in minerals, is not always possible. While a unique relation exists between the wavelength (energy) of X-ray photons and the elements present in the target, no such unique relation exists between the CL emission peak or band energies and the nature of the impurities involved in the CL emission mechanisms. In addition, the CL emission is dependent on the mechanisms of the incident energy dissipation and on the dielectric properties of the crystals.

Correlations have been shown between CL images and the distribution of trace elements detected by means of X-ray spectrometry with the electron probe microanalyzer and with micro-PIXE (proton induced X-ray emission) as discussed (among others) by Rémond *et al.* (1995a) and Yang *et al.* (1992) for the case of zircon ($ZrSiO_4$). Such comparisons between ionoluminescence and trace element distribution with micro-PIXE has been reported by Yang *et al.* (1995). However, these comparisons do not allow one to correlate the detected impurities with the luminescent centers responsible for the CL emission. Although most rare-earth elements (REE) produce sharp CL emission lines, the qualitative interpretation of CL emission spectra for identifying trace elements must be performed carefully.

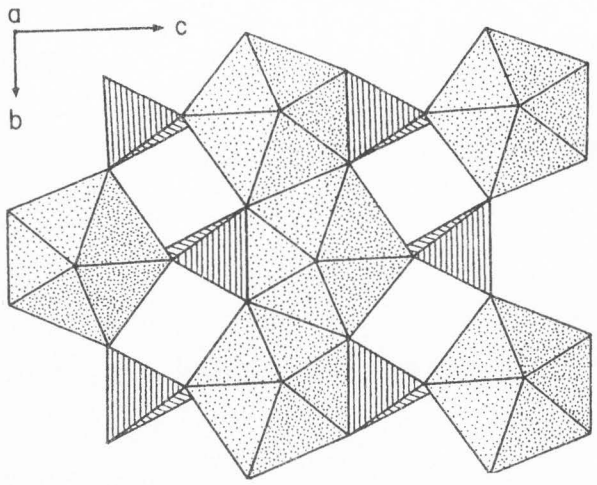

Figure 1. Projection, modified after Speer (1982), of the zircon structure on (100), showing the chains of alternating SiO_4 tetrahedra (hatched) and ZrO_8 triangular dodecahedra (dotted).

Zircon is an accessory mineral widely distributed in igneous, metamorphic and sedimentary rocks. The incorporation of REE ions may result in the emission of complex CL spectra. Dy^{3+} and Tb^{3+} were recognized as the most frequent activators in natural zircons (Mariano, 1988, 1989; Marshall, 1988; Ohnenstetter *et al.*, 1991; Rémond *et al.*, 1992; Yang *et al.*, 1992). Ohnenstetter *et al.* (1991) and Rémond *et al.* (1992) examined zircons originating from a wide range of rock types and observed that their CL spectra belonged to one of two general groups. The first group displays a broad emission band with a maximum in the blue region with superimposed sharp lines that are characteristic of Dy^{3+}. The second group presents a broad yellow/green emission band, the interpretation of which is still not clear.

In the absence of any general theoretical framework for relating CL spectra to crystal impurities, empirical approaches are mainly used and involve two steps: (1) Use of non-destructive analytical techniques in order to have a spatially resolved analysis of the impurity contents within the material; and (2) interpretation of the CL spectra to identify specific impurities, among those detected, which can play a role in the observed luminescence properties. The identification of these elements must be used as a guide for preparing doped synthetic compounds under controlled conditions. However, a complete understanding of CL emission spectra can only be achieved by considering both the impurity related (extrinsic CL) and the lattice defect related CL emission (intrinsic CL).

The identification of REE by means of X-ray spectrometry with the EPMA is difficult because of the low concentrations to be measured and the frequent X-ray peak overlaps of the L or M X-ray lines for these elements. CL spectroscopy of zircon minerals may avoid some of the above limitations and is expected to complement X-ray spectrometry.

It is the objective of this study to grow undoped and REE-doped zircon crystals to be used for obtaining a collection of CL reference spectra characteristic of each REE added into the zircon crystal structure. These materials and their CL spectra, should be a valuable reference for obtaining a reliable relationship between the complex CL emission spectra of natural zircon crystals and the nature of the REE present at trace levels.

In this study, the raw CL data are not corrected for the response function of the instrument and only **qualitative** interpretation of the spectra are considered. The need for applying such instrumental correction factors is discussed after the potential use of the synthetic crystals and their CL spectra for reference materials and a data bank is demonstrated. The dependence of the CL emission properties upon the excitation conditions and the crystallographic orientation of the zircons is important when they are considered as possible standards and this too is investigated.

Structure, Morphology, Zoning and Chemistry of Zircon

Structure

Zircon is an orthosilicate with a body-centered tetragonal unit cell, belonging to the $I4_1/amd$ space group symmetry; optically it is uniaxial positive. Its structure (Robinson *et al.*, 1971; Hazen and Finger, 1979; Robinson, 1979), shown in Figure 1, consists of chains of alternating edge-sharing SiO_4 tetrahedra and ZrO_8 triangular dodecahedra. The chains run parallel to the *c*-axis and are linked laterally by dodecahedra sharing an O-O edge. There is only one crystallographic equivalent position for the zirconium and each Zr is surrounded by eight oxygen atoms at 0.2128 nm, and four at 0.2267 nm (Hazen and Finger, 1979) constituting the triangular dodecahedra.

Morphology and zoning

Morphologically, crystals usually show a combination of prisms and dipyramids, however, some zircons, tabular on {001}, have also been found (Cesbron *et al.*, 1985). A typological classification based on the preferential development of the {100} and {110} prisms or the {101} and {211} dipyramids, which could be correlated to the $(Na_2O + K_2O)/Al_2O_3$ ratio (agpaicity index) and to the temperature has been proposed (Pupin and Turco, 1972, 1975; Pupin, 1976, 1980).

Zircon frequently are inhomogeneous and display complex and sometimes oscillatory chemical zoning, owing to chemical and physical changes in the silicate melt or solution from which they crystallized; identical but simpler zonations can also be found in synthetic crystals growing from a flux. It is also common to observe epitaxial overgrowths around a primary core, representing later generations of zircon and differing in composition.

Chemistry

The theoretical formula, $ZrSiO_4$, of zircon does not reflect the complexity of its chemical composition and, consequently, of its CL emission. A complete solid solution exists between zircon and hafnon $HfSiO_4$ (Correia Neves *et al.*, 1974), however Hf does not exceed 3% in most natural zircons. According to Robinson (1979), this element could concentrate at the rims. Zircons commonly contain not only hafnium but also yttrium, lanthanides, actinides, phosphorous and lead. Usually, yttrium and the heavy rare earth elements (HREE) predominate, as their ionic radius are close to that of Zr^{4+}; nevertheless light rare earth elements (LREE), with a larger ionic radii, can also be present.

These elements are frequently accompanied by phosphorus and this suggest the classical xenotime-type substitution scheme proposed by Dennen and Shields (1956) which implies that Zr^{4+} is replaced by $Y^{3+} + Ln^{3+}$ in the dodecahedral site, whereas P^{5+} replaces Si^{4+} in the tetrahedral site:

$$Zr^{4+} + Si^{4+} \rightleftarrows P^{5+} + REE^{3+} \qquad [1]$$

In most cases, the amount of phosphorus required is not sufficient and several authors suggest that the deficit of charges between Zr^{4+} and REE^{3+} is compensated by the replacement of O^{2-} by $(OH)^-$ in the tetrahedral site (Vinokurov *et al.*, 1971; Caruba *et al.*, 1974, 1975; Medenbach, 1976; Robinson, 1979; Caruba, 1979; Ohnenstetter *et al.*, 1991), according to the formula: $(Zr^{4+}_{1-\epsilon}\ REE^{3+}_{\epsilon})\ (SiO_4)_{1-x}\ (OH)_{4x-\epsilon}\ \square_{\epsilon}$. Caruba *et al.* (1974) even hydrothermally synthesized an hydroxyl zircon with about 10% Dy replacing Zr.

The tetrahedral substitution $[(OH)_4]^{4-} \rightleftarrows [SiO_4]^{4-}$ was first proposed by Frondel (1953) and Frondel and Colette (1957) but fluorine can also be present, replacing the hydroxyl ions (Caruba *et al.*, 1985). Another possibility for high REE concentration is the coupled substitution proposed by Eskova (1959) and Soltnsev and Scherbakova (1974):

$$2\ Zr^{4+} \rightleftarrows (Nb,Ta)^{5+} + REE^{3+} \qquad [2]$$

Y_2O_3 can reach up to 16.5 wt%, however most of the natural zircons do not exceed 3 wt% Y_2O_3. A total of 25 wt% $Y_2O_3 + REE_2O_3$ has been reported by Medenbach (1976) but most of the high REE natural zircons appear as a microscopic mixture of zircon and xenotime. The Y_2O_3 decreases in magmatic zircons from oceanic towards migmatitic granites, whereas HfO_2 shows the opposite trend; thus, the zircons from oceanic granites are characterized by high Y, low Hf, and extremely low U and Th values (Pupin, 1992). Niobium can occur in zircon and attain values up to 5% Nb in the Thor Lake rare-metal deposit (Smith *et al.*, 1991).

Usually the concentration of actinides ranges from 4 to 5000 ppm for U and from 2 to 2000 ppm for Th (Speer, 1982); however, contents up to 6 wt% of total actinides are known. Uranium is incorporated selectively on the {101} and {211} pyramidal and {100} prismatic faces, producing hour-glass and "Maltese cross" structures (Carpena *et al.*, 1987). In actinide-rich zircons, defects are produced by the bombardment induced by the natural radioactive alpha-decay and zircons become progressively amorphous, leading to the aperiodic metamict state (Chakoumakos *et al.*, 1987). When about 20% of the atoms are displaced, the crystal becomes X-ray amorphous (Pellas, 1954).

Materials and Methods

Synthesis of zircons

Zircon was first synthesized by Sainte-Claire Deville and Caron (1858) by heating zirconia at high temperature under a SiF_4 atmosphere. The first lithium molybdate flux-grown zircons were obtained by Hautefeuille and Perrey (1898) and the hydrothermal synthesis of zircon, using silica and zircono-hydroxide gels was first performed by von Chrustschoff (1892). The hydrothermal method (Caruba *et al.*, 1974; Caruba *et al.*, 1988) usually produces very small crystals of about 100 mm and requires the use of a natural crystal as a seed; using a fluoride mineralizer, the size can reach the centimeter range (Dharmarajan *et al.*, 1972; Uhrin *et al.*, 1974). The seed can be a serious problem in that outer parts of the seed can be dissolved (Caruba *et al.*, 1974) before the beginning of the epitaxial growth, and then contaminate the hydrothermal solution with unwanted trace-elements since natural zircons never are chemically pure. We selected the flux method to avoid this problem and the crystals were grown from a flux consisting of equal proportions of Li_2MoO_4 and MoO_3, in which stoichiometric quantities of SiO_2 and ZrO_2 were dissolved after careful mixing; the quantity $SiO_2 + ZrO_2$ represented 1.34% of the flux mass. The purest available products were used; nevertheless ZrO_2 contains up to 470 ppm of P, 93 ppm of Fe, 54 ppm of Ca; 24 ppm of Hf, 6 ppm of Th and less than 5 ppm of Sm. Spectrographically pure REE were usually introduced as oxides, more rarely as carbonate, and were accompanied with ammonium phosphate in order to take into account the xenotime-type substitution:

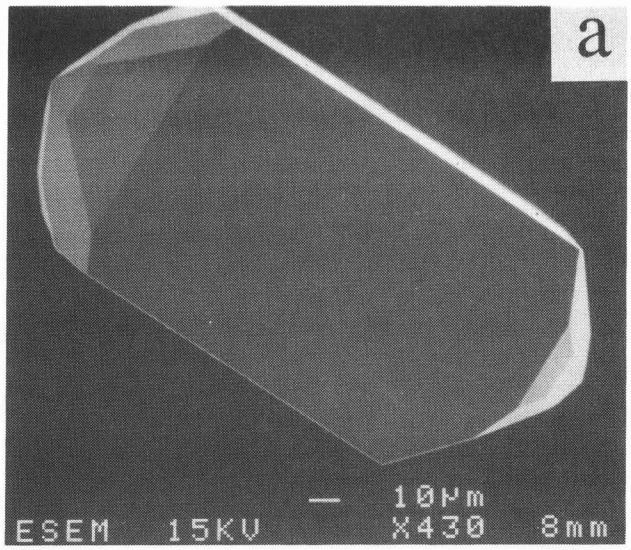

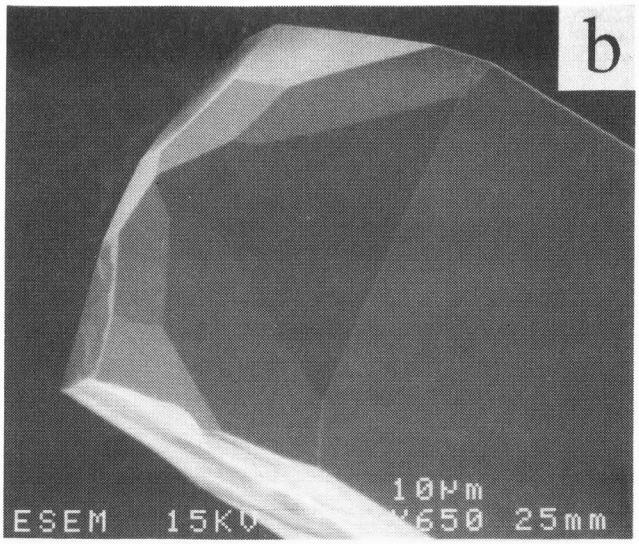

Figure 2. (a) Secondary electron SEM image of a pure synthetic zircon displaying {100}, {101}, {102} and {112}; (b) magnification of the apex with the different pyramids; (c) idealized drawing of a synthetic crystal, with the optical orientation. ϵ corresponds to the extraordinary refractive index and ω to the ordinary refractive index.

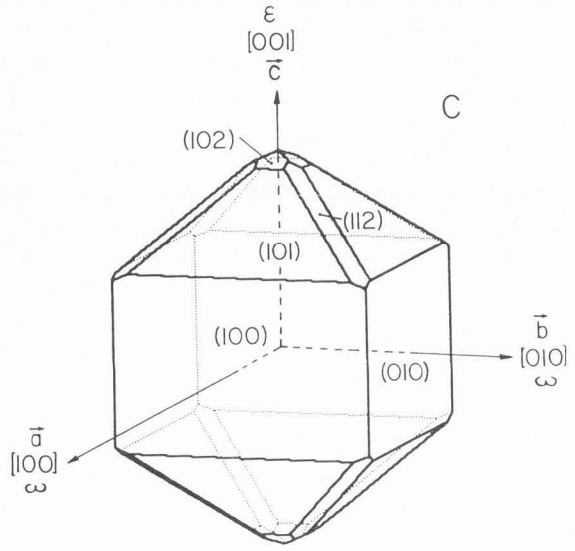

$$Zr^{4+} + Si^{4+} \rightleftarrows P^{5+} + (Y, Ln)^{3+} \qquad [3]$$

Calculated $REE(PO_4)$ represented 6% of the quantity of $SiO_2 + ZrO_2$ introduced in the flux.

The mixture, placed in a platinum crucible, was initially heated at 1125°C for 48 hours in order to ensure a good homogenization, then it was cooled to 900°C with a cooling rate of 1°C/h and subsequently from 900 to 750°C with a cooling rate of 2°C/h. Inside the muffle furnace, the crucibles and their lids were placed inside covered alumina crucibles to minimize the volatilization of MoO_3.

Undoped and doped zircons (doped with Y and all the natural lanthanides, La, Ce, Pr, Nd, Sm, Eu, Gd, Tb, Dy, Ho, Er, Tm, Lu, with or without accompanying phosphorus), were synthesized. Crystals were recovered after dissolution of the flux with a mixture of hot water and hydrochloric acid.

According to Dharmarajan *et al.* (1972), the solubility of zircon at 1200°C in such a flux is only 1.55%. The synthesized crystals can reach a maximum size of 3 mm, as short or elongated {100} prisms displaying the {101}, {102} and {112} dipyramids (Figs. 2a and 2b); the apex of doped crystals is sometimes terminated by a reduced pinacoïd {001}. An idealized drawing of such a crystal in given in Figure 2c. Growth zonation and resorption-recrystallization phenomena (these latter occurring with inopportune accidents such as temporary power failure), similar to those observed in natural crystals, were also produced. The complete batch of $SiO_2 + ZrO_2$ did not entirely crystallize as zircon and Li_2SiO_3 crystals (identified by X-ray diffraction), sometimes present as very tiny inclusions inside the zircons, were also produced. However, with these growing conditions, our crystals usually were clear and of gem quality. Spatially resolved X-ray microanalysis data showed that Hf (in amounts from 200 to 300 ppm), Mn, Cr and Fe (in amounts of 30 to 50 ppm) were present but were homogeneously distributed within all synthetic zircons (Remond *et al.*, 1995b).

Cathodoluminescence spectrometry

Spatially resolved CL spectrometry was performed at room- and low temperature (~ 205K) by means of a CL spectrometer attached to a JEOL JSM 840A SEM, as previously described by Cesbron *et al.* (1993) and Blanc *et al.* (1994). The system includes (Fig. 3):

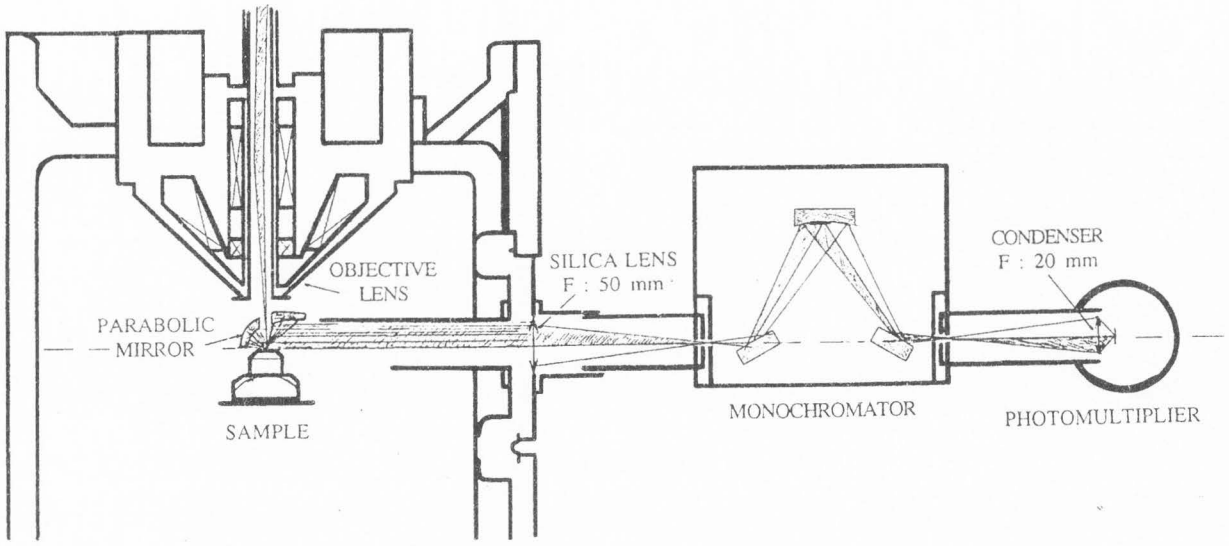

Figure 3. Schematic drawing of the CL spectrometer (without the refrigerating stage) used for this study.

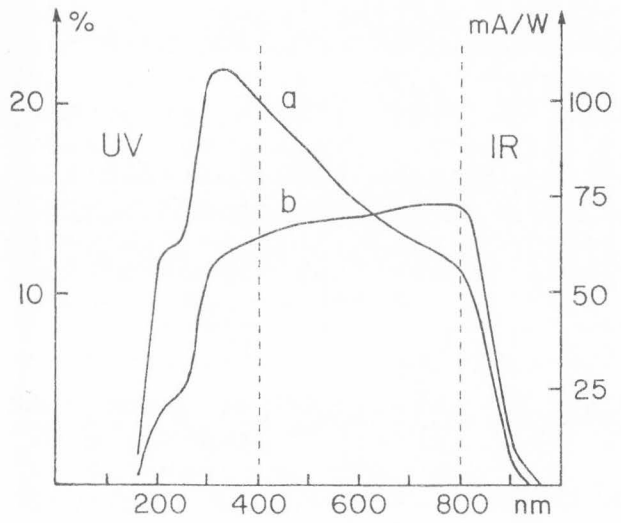

Figure 4. Response curve of the Hamamatsu R636 AsGa photomultiplier as a function of wavelength: (a) quantum efficiency in per cent; and (b) radiant sensitivity in mA/W.

(a) A cooled stage specially built in the laboratory, allowing the sample to reach temperatures near 205K when the crystals were deposited on top of a metallic specimen holder. Temperatures are measured by means of two carbon resistances.

(b) A retractable aluminum plated parabolic mirror placed above the specimen surface; the collected CL emission is focused onto the entrance slit of the spectrometer by means of a silica glass lens as an interface between the specimen chamber and the Jobin-Yvon H10 ultra-violet (UV) spectrometer using a concave holographic grating with 1200 grooves/mm.

(c) A Hamamatsu R636 AsGa photomultiplier with a 650 U response curve as shown in Figure 4.

The wavelength resolution of the spectrometer is 8 nm for a 1 mm width of the slits and 4 nm for 0.5 mm. The analyzed wavelength domain ranges from 200 to 900 nm. Two instrumental anomalies of the spectrometer occur at 500-510 nm and 800-820 nm, respectively, the latter being ten times more significant than the first one. At the present time, the spectra are not corrected for the spectral response function of the spectrometer and detector.

Results

Undoped synthetic zircon crystals

Intrinsic CL emission properties: As shown in Figure 5, the CL emission band occurring in the UV and near visible wavelength region (200 nm $< \lambda <$ 500 nm) consists of 6 bands, labelled a_1 to a_6, at 230 nm (5.390 eV), 290 nm (4.274 eV), 310 nm (3.999 eV), 330 nm (3.756 eV), 355 nm (3.492 eV) and 380 nm (3.262 eV), respectively. For wavelengths greater than approximately 400 nm, the CL intensity continuously decreases to become constant for $\lambda \geq 500$ nm. As the CL spectra was recorded in an analog mode, no spectral decomposition of the partly overlapping bands was performed. However, assuming that the emission bands a_1-a_6 in Figure 5 are symmetrical with the same width, the half-width at half maximum, resulting from the convolution product of the instrumental response function with the natural width of these emissions, can be estimated to be approximately 0.9 eV.

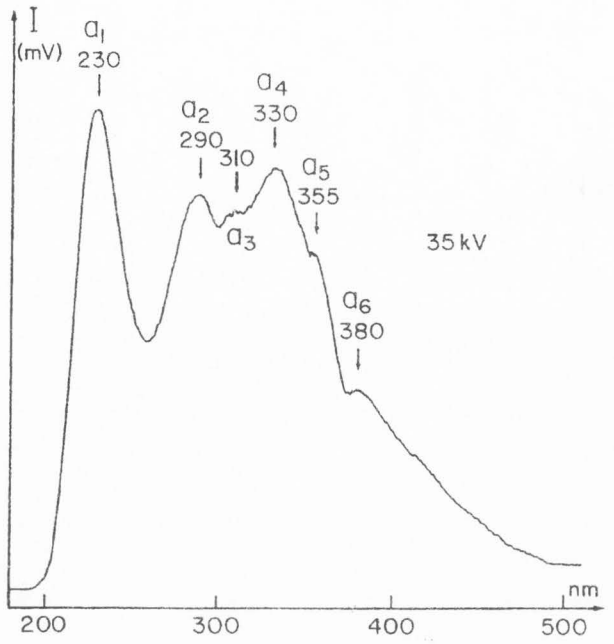

Figure 5. CL spectrum of a pure synthetic zircon, with the positions of the emission peaks constituting the intrinsic band. Analytical conditions: C+Au-Pd coating, temperature ~ 205K, electron beam perpendicular to (100), *c*-axis of the crystal parallel to the mirror axis, accelerating voltage 35 kV, beam current 1 x 10^{-8} A, and 350 mV full scale of the vertical axis.

In a strict sense, intrinsic luminescence (or near edge emission band or also self-activated luminescence) designates the emission resulting from direct recombination of electron-hole pairs through the bandgap of the energy diagram of the crystal. The intrinsic luminescence consists of an emission band centered at an energy $h\nu = E_g$, where E_g is the absorption edge of the material. It is usual to designate all emission characteristic of structural defects in the host lattice as intrinsic. Peaks a_1-a_6 measured at the surface of an undoped zircon crystal are also referred to as host lattice emission or intrinsic emission.

Anisotropy of the intrinsic CL emission bands: Figure 6 shows that the crystal orientation with respect to the electron beam direction and the revolution axis of the mirror strongly influences the relative intensities of the emission bands on the intrinsic emission spectrum. In order to illustrate the anisotropy of the CL emission, the crystals were mounted on the specimen holder in either of the two following orientations: (1) The electron beam is perpendicular to the symmetrically equivalent (100) or (010) faces, the *c*-axis of the crystal being parallel to the mirror axis. This direction, also referred as [001], corresponds to the extraordinary refractive index

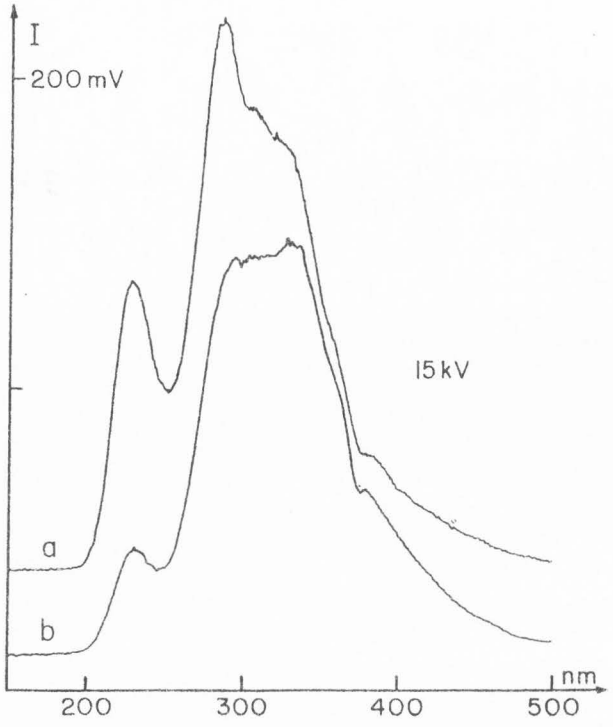

Figure 6. Shape of the intrinsic band of a synthetic pure zircon when the electron beam is perpendicular to (010); (a) *c*-axis (extraordinary refractive index ϵ) is parallel to the mirror axis; (b) the *a*-axis of the crystal (ordinary refractive index ω) is parallel to the mirror axis. Analytical conditions: carbon coating, room temperature, accelerating voltage 15 kV, beam current 1 x 10^{-8} A.

ϵ of a uniaxial positive crystal (Fig. 2c). Sometimes, it is called the "ϵ-orientation". (2) The electron beam is perpendicular to the symmetrically equivalent (100) or (010) faces, the *a*- or *b*-axis of the crystal being parallel to the mirror axis. Both directions, [100] and [010] respectively, correspond to an ordinary refractive index ω of a uniaxial positive crystal. Sometimes, this is called the "ω-orientation".

CL spectra in Figure 6 show the difference between the CL emissions produced with these two orientations, the signal being stronger in the ϵ-orientation (Fig. 6a) than for the case of the ω orientation (Fig. 6b). When turning the crystal by a 20° step around a binary axis (*a*- or *b*- axis, parallel to the electron beam), the CL spectra showed progressive variations of the relative intensities of the emission bands indicating that the luminescent emission has a spatial binary symmetry (we also observed this "polarization effect" for the case of calcite, apatite, etc., unpublished observations). In addition, the CL emission has a revolution symmetry around the fourfold *c*-axis as shown in Figure 7 corresponding to the

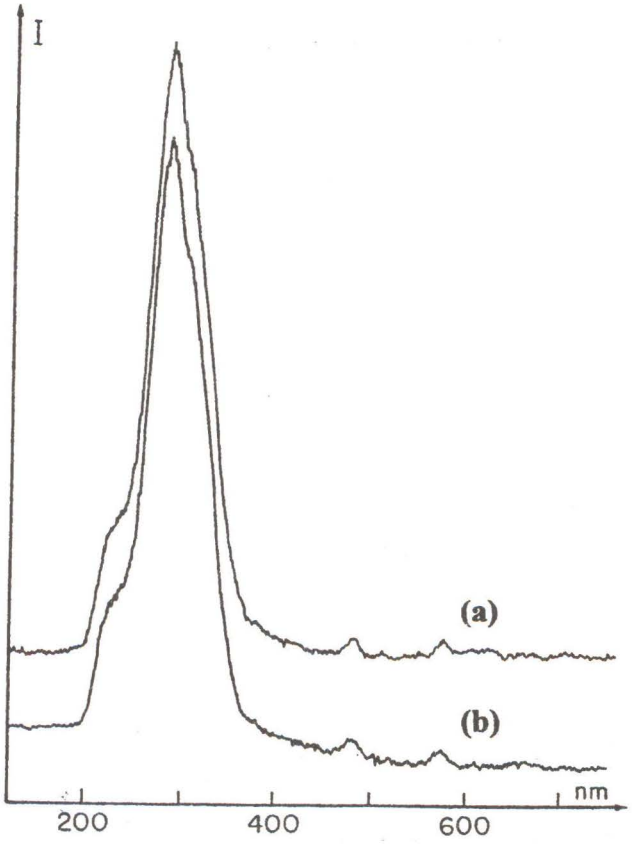

Figure 7. CL emission spectra of a pure synthetic crystal sawed perpendicularly to the *c*-axis and polished. The electron beam is parallel to the four-fold axis [001] of the crystal and the spectra correspond to two ordinary refractive indices (ω) with *a*- and *b*-axes, respectively set parallel to the mirror axis. The CL emission is symmetrical around [001]. Analytical conditions: carbon coating, accelerating voltage 25 kV, beam current 6 x 10^{-8} A.

CL spectrum measured at 205K at the surface of a synthetic crystal sawed perpendicular to the *c*-axis before being polished. For the case of the CL spectra shown in Figure 7, the electron beam is parallel to this axis {i.e., perpendicular to the (001) face} and the two binary axes were successively set parallel to the mirror axis.

Relative intensities of the CL emission bands as a function of the excitation conditions: The intrinsic CL emission bands, measured at 205K, as a function of the incident beam current and a 10 keV electron beam, are shown in Figure 8 for the case of an undoped zircon crystal (possible impurities other than those present in the fluxing oxides were not analyzed in the undoped zircon). The direction of the incident electron beam was normal to the (100) face of the crystal. The intensities of the CL emission bands were measured as the height

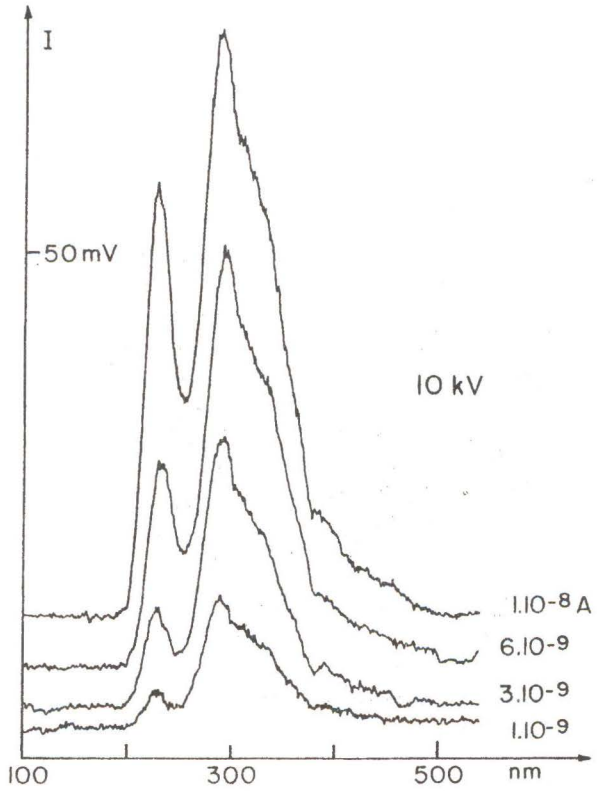

Figure 8. Modification of the intrinsic band shape with the electron beam intensity. Electron beam perpendicular to (100), *c*-axis (ϵ-position) parallel to the mirror axis, accelerating voltage 10 kV, temperature 205K.

---

of the band maximum to the base lines corresponding to the CL intensity for wavelengths shorter than 200 nm. The intensity ratio I_{230}/I_{290} of the emission bands centered at 230 nm and 290 nm respectively increased from 0.28 to 0.74 when the beam current was increased from 1 x 10^{-9} A to 1 x 10^{-8} A.

CL spectra in Figure 9 (ϵ-orientation) and Figure 10 (ω-orientation) illustrate the strong dependence of the crystal orientation and the irradiation dose (3 keV < E < 35 keV and a constant beam current 1 x 10^{-8} A) on the shape and intensity of the intrinsic bands. In order to make the CL emission spectra comparable, only those obtained for incident energies ranging from 3 keV to 12 keV are shown, with the same intensity scale (Figs. 9 and 10). From Figures 9 and 10 (corresponding to CL emissions measured **at room temperature**) it can be seen that the intensity of the peak centered at 230 nm was higher for the case of the crystal in the ϵ-orientation than that observed when the crystal was in the ω-orientation. Furthermore, as shown in Figure 11, the intensity ratios I_{230}/I_{290} were higher for the ϵ-orientation than for the case of the ω-orientation.

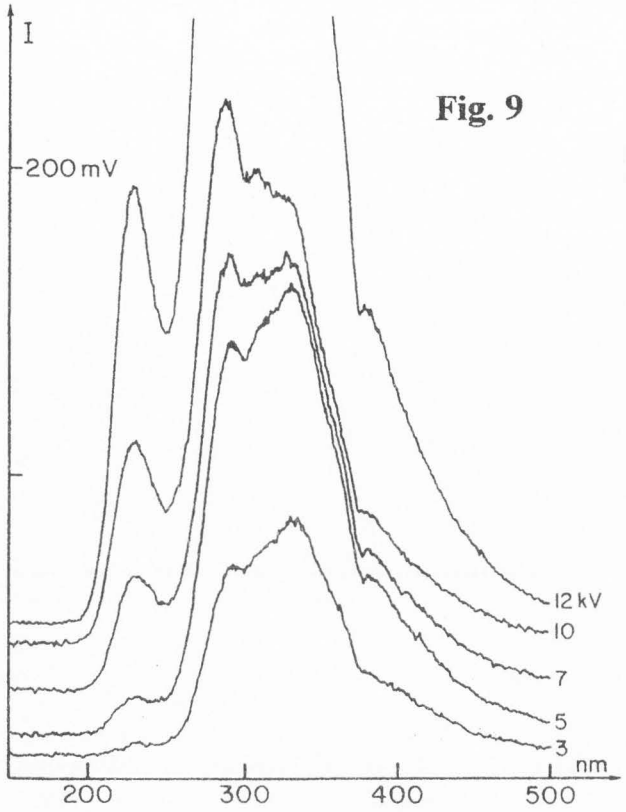

Fig. 9

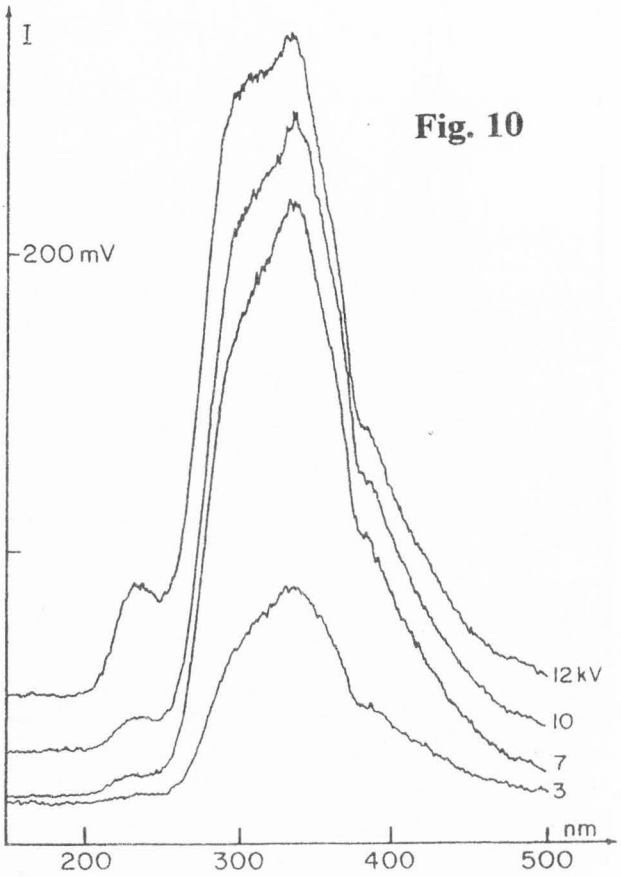

Fig. 10

Figures 9 (at left) and 10 (at right). Modification of the intrinsic band shape with the accelerating voltage. Electron beam perpendicular to the (100) plane; *c*-axis (ϵ-orientation, **Figure 9**) and *a*-axis (ω-orientation, **Figure 10**) parallel to the mirror axis. Beam current: 1 x 10^{-8} A; room temperature.

REE-doped zircon CL spectra

CL emission spectra of zircon doped with a single REE: CL spectra were measured at room temperature and after the specimens were cooled down to approximately 205K successively. No significant changes in the shape of the CL emission spectra were observed as a function of the specimen temperature but only the intensities were found to be higher for cooled specimens than at room temperature. Only spectra measured at a temperature near 205 K are shown. All spectra were obtained at the same excitation conditions, i.e., accelerating voltage: 25 kV; beam current: 1 x 10^{-8} A; magnification: x300; and working distance: 25 mm. The zircon crystals were directly set with Araldite glue on an aluminum plate in order to obtain rapid cooling; no polishing was performed, the "as manufactured" crystal surfaces were carbon coated. As illustrated in the next section, the position of the analyzed crystal with respect to the directions of the electron beam and the mirror revolution

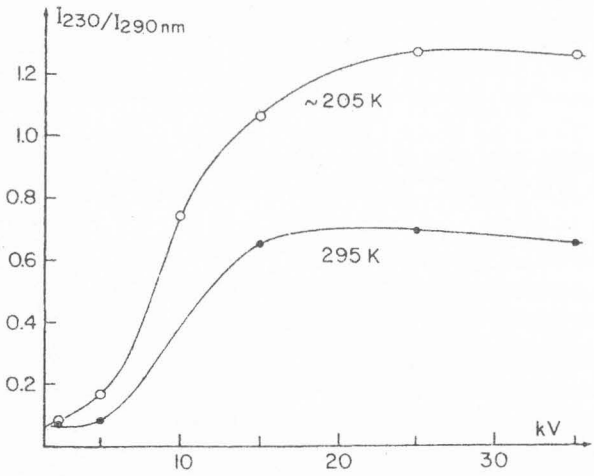

Figure 11. I_{230}/I_{290} intensity ratio for the bands centered at 230 nm and 290 nm as a function of the accelerating voltage measured at room temperature and at 205K. Electron beam perpendicular to (001), *c*-axis parallel to the mirror axis, beam current 1 x 10^{-8} A.

axis respectively can have a marked influence on the shape of a spectrum; so, all spectra shown in Figure 12.1 to Figure 12.14 (presented on pages 44-47 for the ease of comparisons) were obtained with the electron beam perpendicular to the symmetrically equivalent (100) and (010) faces, the *c*-axis of the crystal being parallel to the mirror axis ("ϵ-orientation").

The CL emission spectra of the REE doped zircons in Figure 12.1 to Fig 12.14 exhibit two types of features: (1) broad emission bands occurring in the UV part of the analyzed wavelength domain; and (2) narrow peaks whose positions varied as a function of the nature of the REE ion being incorporated within the zircon crystals. The broad emission band ranging from 200 nm to 300 nm is similar to that observed for the case of the undoped zircon crystals and is intrinsic in origin. The other bands and the narrow peaks of weak intensities (but with positions varying with the nature of the doping element) are thus extrinsic in origin, i.e., are characteristic of the luminescent REE ions.

Some ions, such as Y^{3+}, La^{3+}, Ce^{3+}, Nd^{3+}, Yb^{3+} and Lu^{3+}, do not display such lines but can give, as Y^{3+}, a broad emission band of weak intensity as compared to the intrinsic band (Fig. 12.1).

Only Tm^{3+} (Fig. 12.12) presents a peak at the limit of the visible and infrared (IR) domains but Gd^{3+}, Tb^{3+}, Ho^{3+}, Er^{3+}, and Tm^{3+} present one or several well-defined lines in the UV domain, superimposed on the intrinsic emission band (Figs. 12.7, 12.8, 12.10, 12.10, and 12.12, respectively).

It must also be noted that a small peak, in the range 495-510 nm, is sometimes present on the longer wavelength side of the intrinsic band, mainly when this latter is very important compared to the characteristic lines: it can be seen for La^{3+} (Fig. 12.2a), Ce^{3+} (Fig. 12.2b), Sm^{3+} (Fig. 12.5), Gd^{3+} (Fig. 12.7) and Ho^{3+} (Fig. 12.10). This peak is probably due to an instrumental aberration or to a 4f transition of an ubiquitous REE impurity.

Influence of the crystal orientation on the REE CL emission line intensities: The influence of the crystal orientation on the shape and intensity of CL peaks is illustrated in Figure 13 for the case of the Dy-doped zircon. The two major characteristic CL emission peaks are centered near 485 nm and 580 nm respectively. As shown in Figure 13 the relative intensities of the 485 nm and 580 nm peaks remain in the same order of magnitude for both orientations of the crystal, i.e., the ϵ or the ω refractive index being parallel to the mirror axis successively. Consistent with high resolution CL emission spectra reported by Rémond *et al.* (1992) for the case of natural zircon containing Dy as impurity, the major CL emission peaks at 485 nm in Figure 13 for the case of the synthetic Dy-doped zircon can easily be resolved into a triplet with maxima at 475, 485, and 490 nm ($\pm$ 3 nm). When the crystal has its ordinary refractive index ω (*a*- or *b*-axis) parallel to the mirror axis (Fig. 13b), the intensity of the peak centered at 485 nm is lower than that measured with the extraordinary refractive index ϵ (*c*-axis) parallel to the mirror axis (Fig. 13a). Furthermore, the three features are better resolved in the first orientation than the second one. When the crystal has its ordinary refractive index ω (*a*- or *b*-axis) parallel to the mirror axis (Fig. 13b), the intensity of the peak at 580 nm (consisting of a doublet) is also lower than that measured when the extraordinary refractive index ϵ (*c*-axis) is orientated parallel to the mirror axis. In addition, for the latter case, the two features are no longer resolved.

The CL spectrum of the Eu^{3+}-doped zircon exhibits two major peaks at 595 and 710 nm respectively as shown in Figure 14. The shape of the peak at 595 nm is asymmetrical. Depending on the crystal orientation with respect to the mirror axis, the asymmetry of the 595 nm band occurs on the long wavelength side (low energy side) or on the short wavelength side (high energy side) of the peak. The asymmetry results from the presence of two incompletely resolved features labelled α_1 and α_2 in Figure 14 with relative intensities α_1/α_2 varying with the crystal orientation. As shown in Figure 14 the α_1/α_2 is higher when the *c*-axis is parallel to the mirror axis than for the case of the *a*-axis perpendicular to that direction. The peak centered at 710 nm also consists of a doublet marked β_1 and β_2 in Figure 14. However, the intensity ratio β_1/β_2 varies as a function of the crystal orientation but, in an opposite direction than for the case of the α_1/α_2 intensity ratio, i.e., the β_1/β_2 intensity ratio is the highest when the *a*-axis is parallel to the mirror axis. These intensity variations lead to an apparent shift in the position of the 595 nm and 710 nm peaks when the occurrence of fine structures is omitted.

Another example of such an inversion can be seen in the Sm^{3+} spectra (Figs. 15a and 15b). Obviously, if a spectrometer does not have sufficient resolution, this can lead to discrepancies on the maximum peak position if the crystal is randomly oriented as is the case in polished thin sections.

Again, the increase of the CL intensities measured for the ϵ-orientation with respect to that obtained for the case of the ω-orientation is observed when comparing the intensities of the peaks at 550, 660, 670, 730 and 760 nm measured for the case of the Ho^{3+}-doped zircon crystal (Fig. 16). It is noticeable that the intensity of the peak at 730 nm varied in such a way that it is no longer detected when the *c*-axis is parallel to the mirror axis. All peaks shown on the CL emission spectra of the Ho^{3+}-doped zircon (Fig. 16) exhibit fine structures with

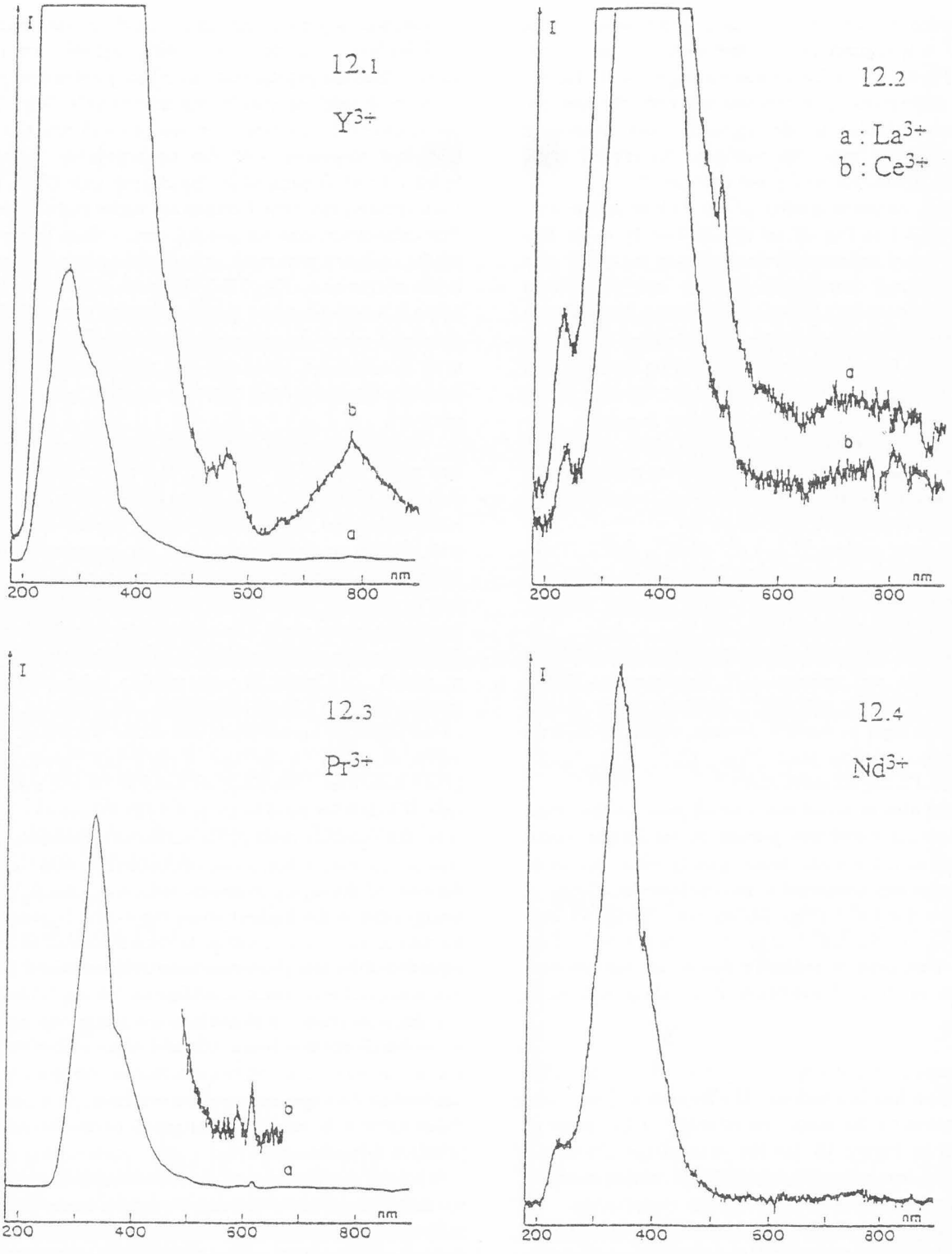

Figures 12.1 to 12.14 (on pages 44-47). All the spectra were obtained with the following analytical conditions: carbon coating, temperature 205K, electron beam perpendicular to (100), *c*-axis (extraordinary refractive index ϵ) of the crystal parallel to the mirror axis, accelerating voltage 25 kV, beam current 1 x 10^{-8} A. All the crystals were doped with REE^{3+} + P^{5+} with the exception of Ho^{3+}. **Figure 12.1.** Zircon doped with Y^{3+}: (a) vertical axis: 250 mV at full scale; (b) 50 mV. **Figure 12.2.** Zircon doped with: (a) La^{3+}, 25 mV; and (b) Ce^{3+}, 25 mV. **Figure 12.3.** Zircon doped with Pr^{3+}: (a) 250 mV; (b) 25 mV. **Figure 12.4.** Zircon doped with Nd^{3+}, 50 mV.

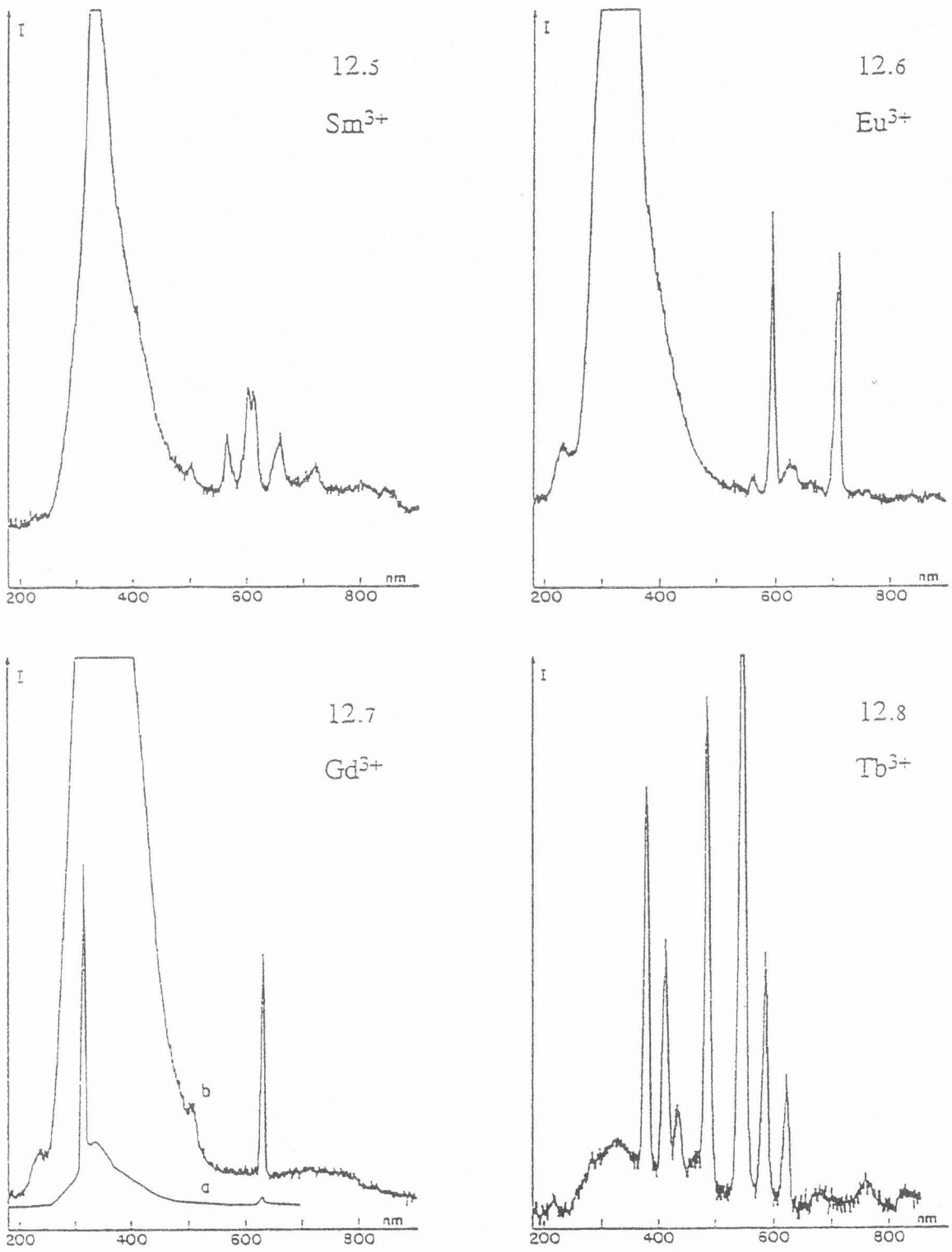

Figure 12.5. Zircon doped with Sm^{3+}, 50 mV. **Figure 12.6**. Zircon doped with Eu^{3+}, 50 mV. **Figure 12.7**. Zircon doped with Gd^{3+}: (a) 1000 mV; (b) 50 mV. The peak at 630 nm may be attributed to a second reflection order. **Figure 12.8**. Zircon doped with Tb^{3+}, 25 mV.

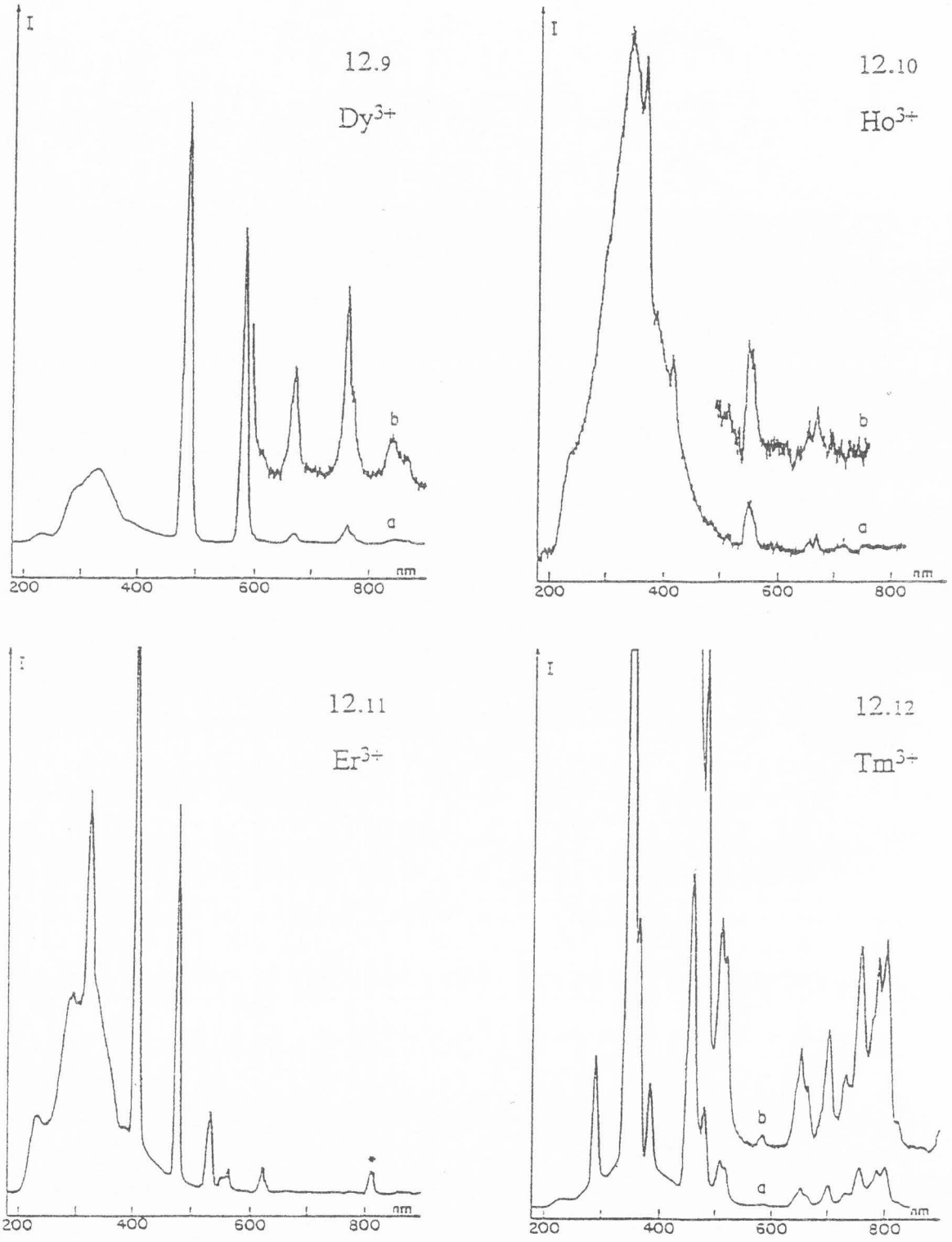

Figure 12.9. Zircon doped with Dy^{3+}: (a) 500 mV; (b) 50 mV. **Figure 12.10**. Zircon doped with Ho^{3+}: (a) 50 mV; (b) 25 mV. **Figure 12.11**. Zircon doped with Er^{3+}, 250 mV. The peak marked by an asterisk is probably due to an instrumental anomaly. **Figure 12.12**. Zircon doped with Tm^{3+} (without P^{5+}): (a) 500 mV, 1.10^{-9} A; (b) 100 mV, 1×10^{-9} A.

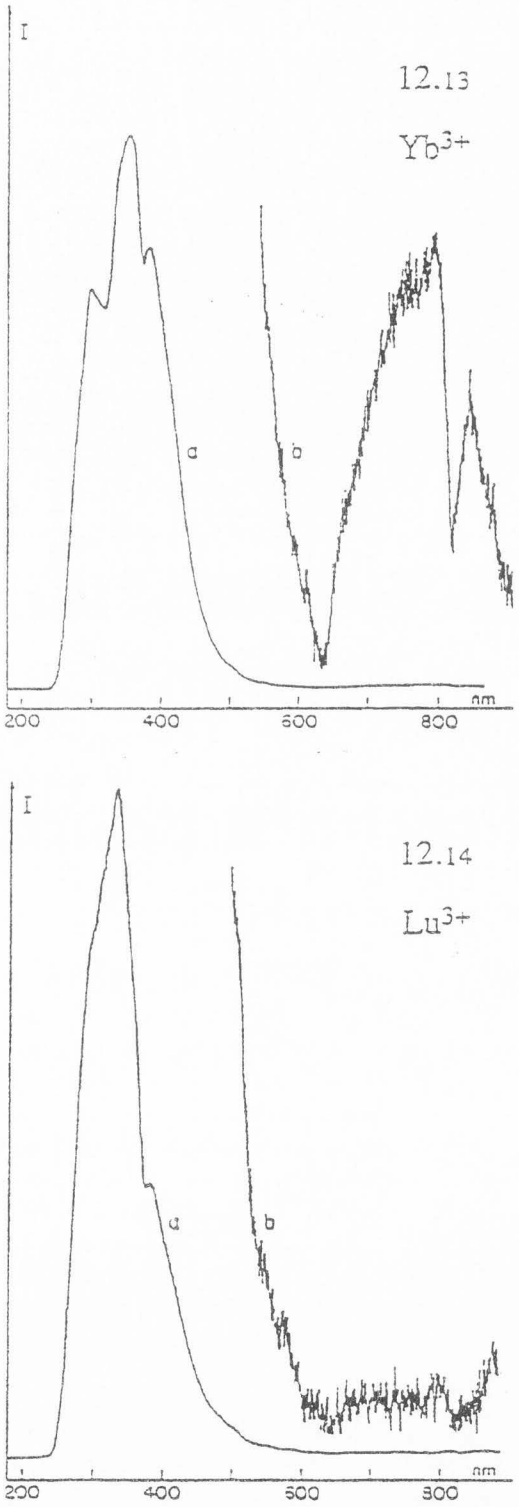

Figure 12.13. Zircon doped with Yb^{3+}: (a) 5 V, (b) 50 mV. **Figure 12.14.** Zircon doped with Lu^{3+}, (a) 1 V, (b) 50 mV.

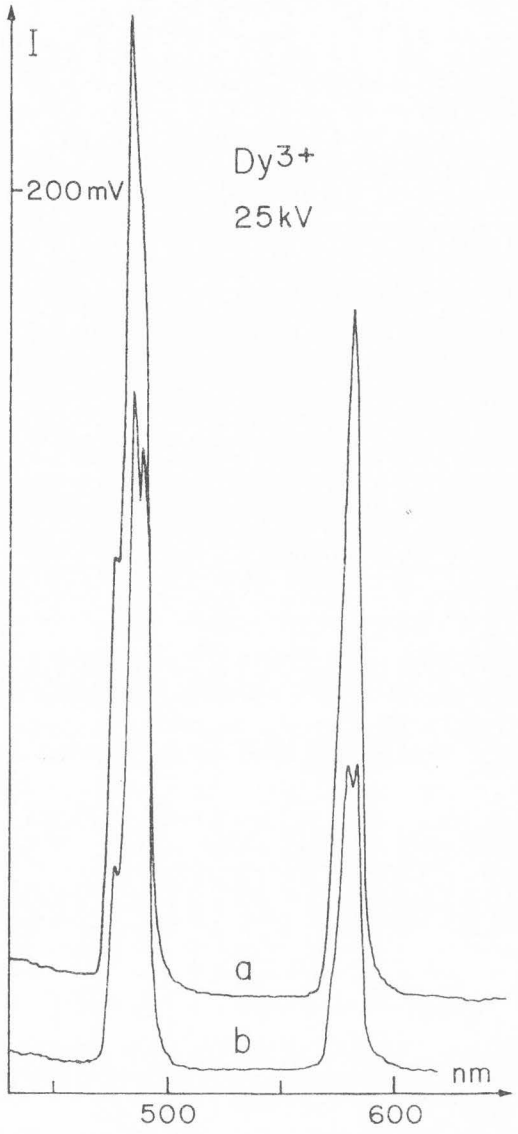

Figure 13. Spectra of a zircon doped with Dy^{3+} + P^{5+}, showing the fine structure of the emission peaks and the influence of the crystal orientation: (a) *c*-axis [001] (extraordinary refractive index ϵ) parallel to the mirror axis; (b) ordinary refractive index (ω) parallel to the mirror axis. Analytical conditions: electron beam perpendicular to (100), accelerating voltage 25 kV, beam current 1 x 10^{-8} A, 205 K.

---

intensities varying as a function of the crystal orientation. The intensities are strongly dependent on the orientation, the CL emission is stronger when the crystal has its *a*-axis (ω) parallel to the mirror axis (Fig. 16b). This is also unusual as the signals in the "ϵ-orientation" are also strong. Not only the "intensity inversion" is evident but a small CL peak appears when the crystal has its *a*-axis parallel to the mirror axis (Fig. 16b).

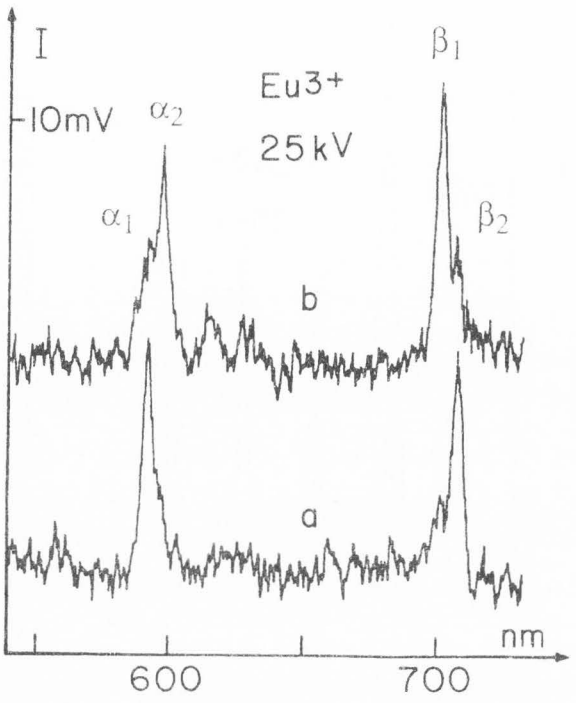

Figure 14. Spectra of a zircon doped with Eu^{3+} + P^{5+} showing the intensity inversion for some doublets: (a) *c*-axis parallel to the mirror axis; (b) *a*-axis parallel to the mirror axis. Analytical conditions: electron beam perpendicular to (010), beam current 1 x 10^{-8} A, accelerating voltage 25 kV, temperature 205 K.

The Data Base

All specimens of either undoped or REE^{3+}-doped zircon crystals exhibited broad CL emission bands in the UV and blue domains. These emission bands must be associated with inherent defects characteristic of the matrix while the narrow emission peaks observed for the case of the REE doped zircons are extrinsic characteristic CL emissions. The term intrinsic was used to designate the luminescence involving lattice defects or impurities accidentally introduced during the manufacture of the crystal (purity of the starting products, nature of the crucible, etc.) and which are different from those specifically added to play the role of activator of the luminescence of the crystal. The ambiguity resulting from the use of intrinsic emission instead of host lattice emission or self-activated emission is discussed in the next paper of this volume (Rémond *et al.*, 1995b).

The intrinsic CL emission spectra (Fig. 5) exhibited bands centered at 230, 290, 310, 330, 355, and 380 nm. The envelope of these emission peaks has a shape very similar to that reported by Votyakov *et al.* (1985) for the case of X-ray induced luminescence of synthetic zircons grown from solution in a melt and under hydrothermal conditions.

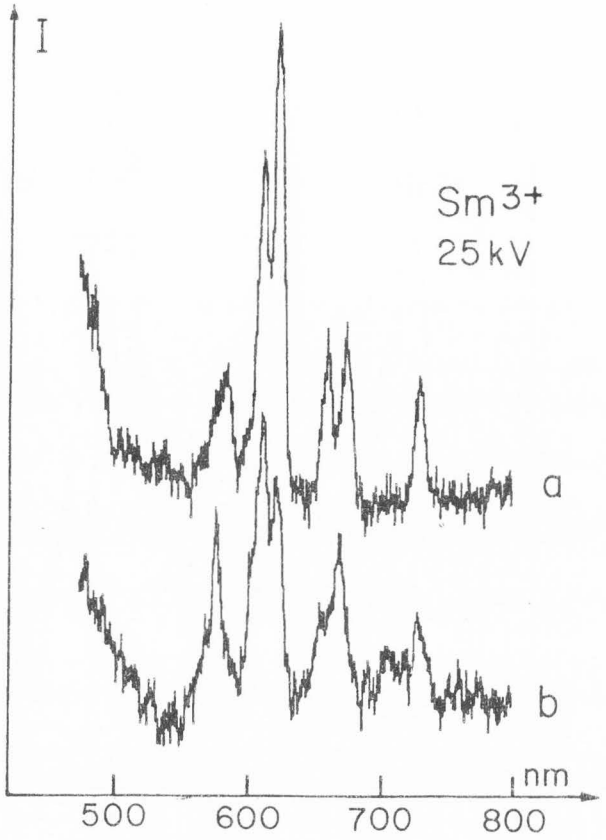

Figure 15. Spectra of a zircon doped with Sm^{3+} + P^{5+}, showing the influence of the crystal orientations: (a) *a*-axis parallel to the mirror axis; (b) *c*-axis parallel to the mirror axis. Analytical conditions: electron beam perpendicular to (010), beam current 1 x 10^{-8} A, accelerating voltage 25 kV, temperature 205K.

The peak centered at 230 nm (5.39 eV) labelled a_1 in Fig. 5 may result from several mechanisms. This position corresponds to the weak peak occurring on the quantum efficiency and sensitivity curves of the detector (Fig. 4). Although an instrumental artefact cannot be completely neglected, the peak at 230 nm is significant and must be regarded as being characteristic of the CL emission of the zircon crystals. This assumption is supported by the change in intensity of that peak as a function of the incident energy (Fig. 11) and beam current (Fig. 10), of the temperature and the incorporation of the REE activators (Fig. 12.1 to 12.14). For zircon, the bandgap is 5.4 eV as reported by Fielding (1970). In addition, the 5.39 eV (230 nm) value of the emission band a_1 in Figure 5, is very close to the measured optical absorption band (Cesbron *et al.*, 1993). Thus, it is tempting to relate the emission peak we measured at 230 nm with the near band edge emission, e.g., the direct recombination of electron-hole pairs from the conduction band. This value of 5.39 eV for the band gap is close

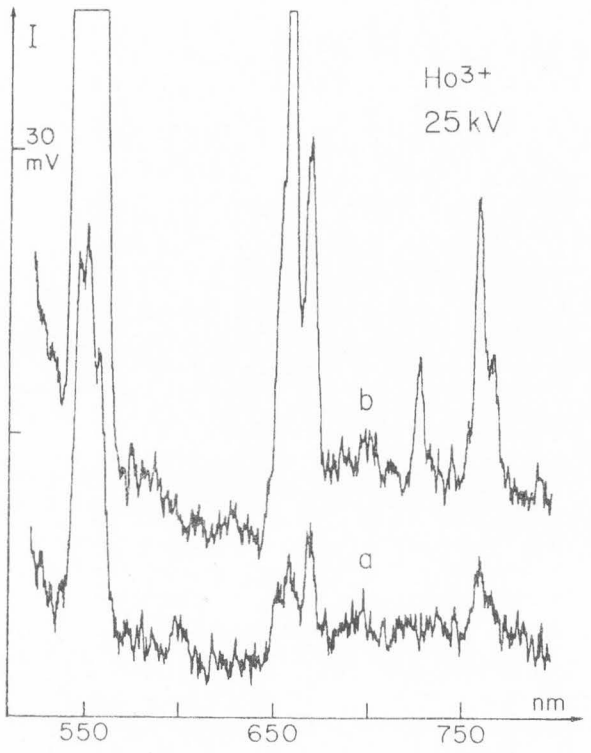

Figure 16. Spectra of a zircon doped with Ho^{3+} + P^{5+} showing the influence of the crystal orientation (fine structure, etc.): (a) *c*-axis parallel to the mirror axis; (b) *a-axis* parallel to the mirror axis. Note the appearance of a small peak at ~ 730 nm. Analytical conditions: electron beam perpendicular to (010), beam current 6 x 10^{-8} A, accelerating voltage 25 kV, temperature 205K.

---

to that for diamond which is a semiconductor and a higher value should be expected for an insulating silicate mineral. A possible explanation is that the observed peak centered at 230 nm should be the tail of an emission band occurring at shorter wavelengths which are not detected with the photomultiplier used.

The peak maximizing at 230 nm extends from ~ 200 nm to ~ 260 nm, a wavelength domain corresponding to the emission bands at 255 and 265 nm reported by Votyakov *et al.* (1985) as being impurity related, the intensities of these bands depend upon the synthesis conditions and the addition of KF, NaF and CaF_2 into the charge. Li originating from the flux and the residual impurities in the ZrO_2 powder used to prepare our crystals may play a role in the luminescent centers associated with the CL emission bands in Figure 5; the presence of P^{5+} into the flux may contribute to the intrinsic emission bands we observed in the present study. The presence of P^{5+}, added to the flux for maintaining the charge balance, leads to a change of the shape and the

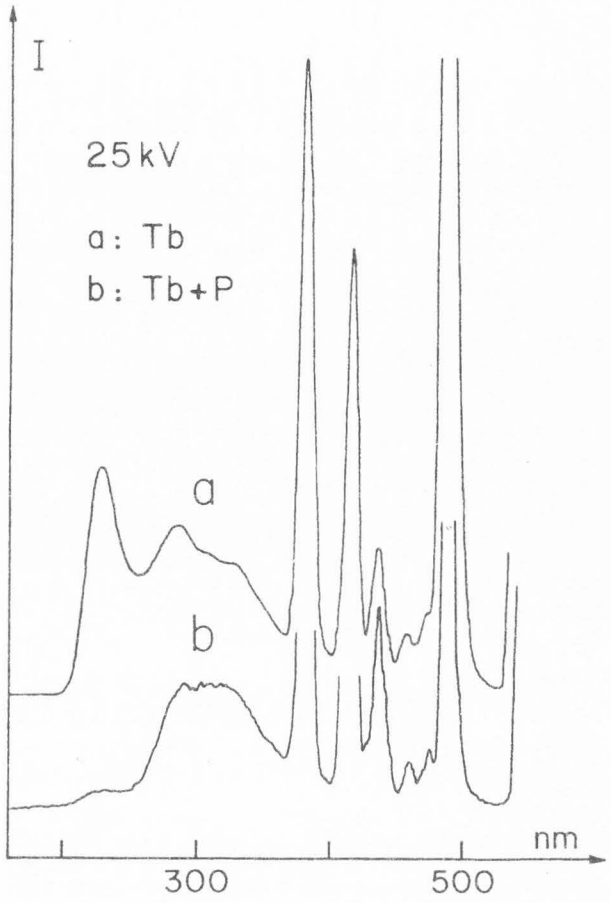

Figure 17. Influence of the doping elements on the intrinsic band (200-360 nm): (a) crystal with Tb^{3+}; (b) crystal doped with Tb^{3+} + P^{5+}. Analytical conditions: electron beam perpendicular to (100), accelerating voltage 25 kV, beam current 1 x 10^{-8} A, 205K, *c*-axis (extraordinary refractive index ϵ) parallel to the mirror axis.

---

intensity of the intrinsic bands but the positions of the CL emission peaks characteristic of a REE^{3+} ion remain unchanged (at least accounting for the energy resolution of the spectrometer used) as illustrated in Figure 17 for the case of the Tb^{3+}-doped crystals. The absence of P^{5+} enhances the intrinsic band, particularly the first peak at 230 nm (Fig. 17a) which barely shows up when P^{5+} is present in the melt (Fig. 17b).

The peaks labelled a_2 to a_6 in Figure 5 are also consistent with data reported in the literature. Luminescence emission bands occurring near 290 nm and 350-380 nm have been reported by Iacconi and Caruba (1980, 1984) studying the thermoluminescence of synthetic zircons. An emission band centered at 280 nm was not assigned by Votyakov *et al.* (1985) while this broad asymmetrical band with many shoulders was attributed to the presence of OH^- groups by Iacconi and

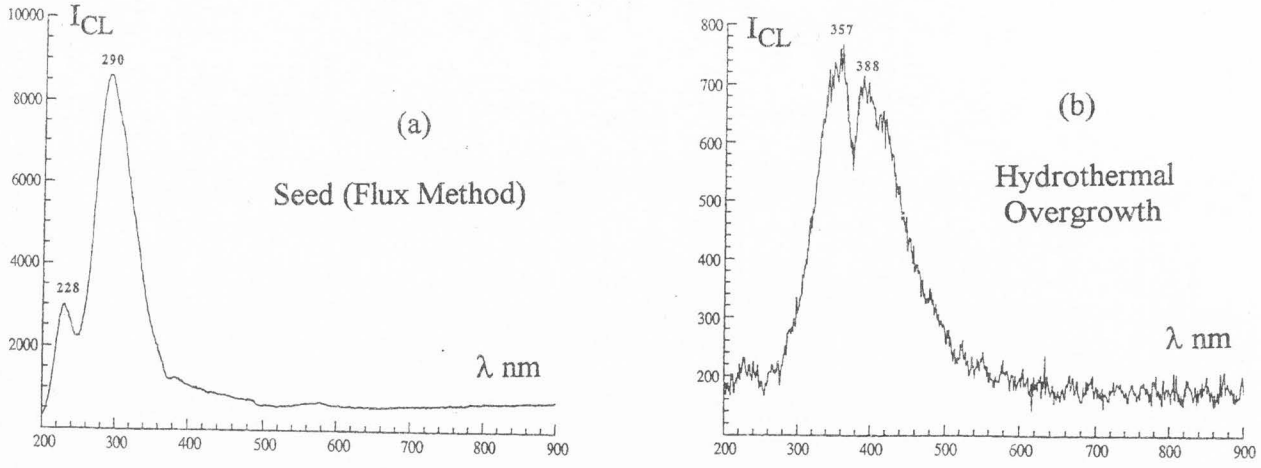

Figure 18. CL emission spectrum of synthetic zircons as a function of the synthesis procedure: (a) crystal prepared according to the flux method, and (b) hydrothermal overgrowth around a seed prepared as in (a). Differences in the intensities may result from the difference in the nature of the recombination centers.

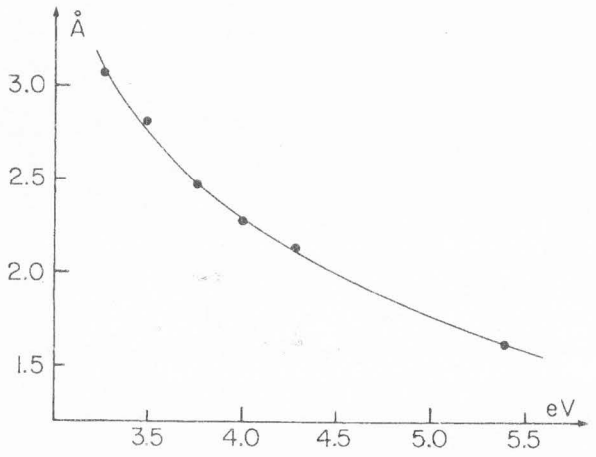

Figure 19. Energy positions of the CL intrinsic emission bands as a function of the interatomic distances for a pure zircon.

Caruba (1977) studying natural and synthetic zircon crystals. No IR spectrometry measurements were performed on the zircons in the present study. The presence of small amounts of OH^- groups cannot be completely excluded, however, the emission band we observe at 290 nm is probably impurity related, inherent to the zircon lattice or synthesis conditions. The emission bands extending from ~ 350 to ~ 380 nm have been reported by Votyakov *et al.* (1985) and related to the decay of excitonic states associated with inherent defects or impurities such as Ti^{4+}. As reviewed by Iacconi (1995), the bands between 340-380 nm should be specific of the excitation of Si-O-Zr chains.

Votyakov *et al.* (1985) showed that the relative intensities of the intrinsic emission bands varied as a function of the temperature of the measurement and the procedure used for preparing the synthetic zircons. The effect of the procedure used on the CL properties was investigated by comparing undoped crystals prepared according to the flux method as described above with the hydrothermally grown crystals (prepared according to the procedure of Caruba *et al.*, 1988). The seed was an undoped zircon prepared using the flux method without the addition of ammonium phosphate. The CL emission spectrum of the seed in Figure 18a exhibits the two intrinsic emission bands centered at 228 nm and 290 nm. The CL spectrum for the hydrothermally grown crystal in Figure 18b shows a shift of the host lattice emission bands towards longer wavelengths with respect to the band positions for the pure zircon used as a seed. For the hydrothermally grown crystal, the two host lattice emission bands were measured at 357 and 388 nm. Differences in intensities probably result from the nature of the defect centers as a function of the crystal growth conditions.

The UV emission is complex and is observed for a large number of silicate minerals which all contain $(SiO_4)^-$ groups, but the origins of the various features are still in doubt. As shown in Figure 19, the energies of the CL intrinsic bands we measured in the present study (Fig. 5) are related to the interatomic distances in a pure zircon given in Table 1 according to Hazen and Finger (1979). This observation in Figure 19 tends to support the view that the UV intrinsic emission is a host lattice emission resulting from the addition of impurities or possibly induced by electron bombardment. The relationship shown in Figure 19 could be used in the future

Table 1. Relation between the energies of the "intrinsic band" peaks and the interatomic distances (Hazen and Finger, 1979) in a pure synthetic zircon.

λ (nm)	E (ev)	distance (nm)	nature and multiplicity of the bonds
230	5.391	0.1623	Si - O [4]
290	4.276	0.2128	Zr - O [4]
310	4.000	0.2267	Zr - O [4]
330	3.758	0.2430	O - O [2][1]
330	3.758	0.2471[5]	
330	3.758	0.2491	O - O [4][2]
355	3.493	0.2749	O - O [4][3]
355	3.493	0.2810[5]	
355	3.493	0.2840	O - O [8][4]
380	3.263	0.3068	O - O [4][4]

[1]Edge shared between a SiO_4 tetrahedron and a ZrO_8 dodecahedron. [2]Edge shared between two dodecahedra;
[3]Unshared edge in a tetrahedron; [4]Unshared edge in a dodecahedron;
[5]average of two distances.

Table 2. Positions (λ in nm) of the CL emission peaks for the different REE in synthetic zircons. Values in bold characters correspond to major peaks; values in italic characters correspond to very weak peaks; values separated by a dash indicate that the peaks contain several incompletely resolved features.

Doping ions	Positions
Y^{3+}	none
La^{3+}	none. The peak at approximately 500 nm (490 to 510 nm) is probably an instrumental anomaly.
Ce^{3+}	none. The peak at approximately 500 nm (490 to 510 nm) is probably an instrumental anomaly.
Pr^{3+}	595, **620**
Nd^{3+}	none for the analyzed specimen but found at 880 nm in natural zircons.
Sm^{3+}	575, **610-620**, 655-670, 725. The peak at 500 nm is probably an instrumental anomaly
Eu^{3+}	560, **595**, 620-635, **710** (705-710)
Gd^{3+}	**315**, *630*. The peak at 505 nm is probably an instrumental anomaly.
Tb^{3+}	**385**, 415, 440, **490**, **550**, 590, 625, *655-675-685*, *765*, *835*
Dy^{3+}	**485** (475-485-490), **580** (580-585), *665*, *755*, *840*
Ho^{3+}	**550** (545-550-560), 660-670, 760
Er^{3+}	**325**, **405**, **480**, 530, 550-560, 620. The peak at 810 nm is probably due to an instrumental anomaly
Tm^{3+}	290, **345**-360, 380, **455**-480, 510-520, 580, 650-665, 700, 730, 755, 790-800
Yb^{3+}	none
Lu^{3+}	none

for a better understanding of the intrinsic emission of most silicate minerals.

According to Monod-Herzen (1966), La, Ce, Yb and Lu ions lead to broad emission bands and only the Sm, Eu, Gd, Tb, and Dy ions have CL spectra exhibiting narrow lines when present either as major components or present as impurities in the minerals. For the case of Pr, Nd, Ho, Er and Tm, the narrow luminescent lines are produced when these elements are present in small amounts within the crystals. The positions of the narrow peaks measured at the surface of the synthetic REE doped zircons, in the present study, are reported in Table 2. The transitions corresponding to characteristic lines of Dy^{3+}, Tb^{3+}, Er^{3+} and Sm^{3+} have been indexed (Cesbron *et al.*, 1993) by comparison with the thermoluminescence (TL) spectra of zircons doped with the same elements (Jain, 1978; Marfunin, 1979; Iacconi and Caruba, 1980; Kirsh and Townsend, 1987). Owing to the many transitions between energy levels, the REE characteristic spectra are complex and many apparently single peaks, are multiplets as previously illustrated by Hanchar and Marshall (1995) and by Rémond *et al.* (1992) using a CL spectrometer with a higher wavelength resolution than that used in the present study.

As reported in Table 2, no characteristic narrow peaks are observable for Dy^{3+} as would be expected according to Monod-Herzen (1966), or from our previous unpublished CL observations of different Nd doped synthetic phosphate minerals showing the characteristic Nd CL lines occurring near 800 nm. In addition, Nd was not detected by means of EPMA or micro-PIXE (Rémond *et al.*, 1995b) indicating that if Nd was incorporated within the synthetic zircon, its concentration should be below the detection limit of the analytical method used. Thus, it is reasonable to postulate that the Nd was not present at sufficient concentration to provoke detectable characteristic CL emission lines and that the observed emission bands on the CL spectra in Figure 12.4 result from lattice defects rather than being related with a REE luminescent ion. Nevertheless, the characteristic Nd^{3+} emission lines can be observed at 811 nm and 880 nm ($I_{811}/I_{880} = 0.2$) in natural zircons containing Nd at concentration level of at least 900 ppm. These emission lines are also present in Nd-doped chloroapatites ($Ca_5(PO_4)_3Cl$) and anhydrites ($CaSO_4$).

Ce^{3+} is also known to give an emission band in several minerals and we observed such a band in Ce^{3+} doped synthetic apatites (350-380 nm) and anhydrite (306-327 nm). In synthetic zircons, the maximum of the band at 335 nm (see Fig. 12.2) is probably associated with the intrinsic emission band rather than with the characteristic Ce emission although this element was detected by micro-PIXE at concentration levels of about 400 ppm (Rémond *et al.*, 1995b). At such low concentrations, the characteristic CL emission of the Ce doping ions is hidden by the intense intrinsic emission band of the zircon crystals.

Conclusions

Based on the data available in the literature and accounting for the instrumental factors and excitation conditions, the so-called intrinsic emission extending within the UV-blue parts of the spectrum for undoped and REE^{3+}-doped zircons analyzed in the present study can be reasonably associated with defects or impurities inherent to the zircon crystals. However, although the addition of P^{5+} ions for preparing the synthetic zircons probably have a role in the intrinsic emission, the nature of the luminescent centers responsible for the zircon intrinsic emission band is still unclear.

The comparisons between the observed CL emission bands in the present study and the data available in the literature are difficult for the following reason: (1) the shape of luminescence spectra varies as a function of specimen preparation and, even for the same method of preparation, large discrepancies may occur between several crystals originating from the same batch; (2) there is a lack available information on the resolution, the response function and the calibration of the spectrophotometers used. As an example, Hanchar and Marshall (1995) reported that CL spectra for a synthetic Dy-doped zircon, analyzed by nine laboratories, exhibited large differences, e.g., the most intense peak was measured between 476.3 nm and 489 nm and was described either as a single peak or as a multiplet containing eight features; (3) peak shifts and relative intensity changes may occur as a function of the nature of the excitation and crystallographic orientation.

Consequently, the deviations between our observed band positions and those reported in the literature may be due to the different sources, i.e., electron bombardment in the present study, X-ray and photo-excitation in Votyakov *et al.* (1985, 1986), and thermal excitation in Iacconi and Caruba (1984). In fact, CL emission can result from the excitation by the primary and secondary electrons, excitation by the generated X-ray photons within the target, by the electrical field resulting from charge trapping and by the temperature increase during the electron bombardment of the specimen. As a consequence, the luminescence yield and the shape of the emission distribution will depend upon the preferential excitation process within the crystal irradiated by the incident electron beam. For the reasons mentioned above, the luminescence spectrum of a crystal containing several luminescent ions may not be the sum of the luminescence spectra of same crystals containing individual impurities. This is in contrast to the case for the

X-ray spectrum of a specimen, which is the sum of the X-ray spectrum of each element contained within a compound. Thus, the mechanisms of luminescence in crystals may lead to complex spectra consisting of many bands and/or narrow peaks whose wavelengths and intensities depend on overall properties of the mineral (i.e., its nature, chemical environment and concentration of the ions, point lattice defects, etc.). In addition, the experimental data should be corrected for the response function of the equipment.

Acknowledgements

The authors thank Dr. R. Baumer (Université de Nice, France) for preparing the hydrothermally grown synthetic zircon. This research was partially supported by the D.B.T. - I.N.S.U. (C.N.R.S.) grant 4/06-4.15 to D.O. and F.C.

References

Blanc P, Arbey F, Cros P, Cesbron F, Ohnenstetter D (1994). Applications de la microscopie électronique à balayage et de la cathodoluminescence à des matériaux géologiques (sulfates, carbonates, silicates). (Applications of scanning electron microscopy and cathodoluminescence to geological materials (sulphates, carbonates, silicates)). Bull. Soc. Géol. Fr. **165**, 341-342.

Carpena J, Gagnol I, Mailhé D, Pupin JP (1987). L'uranium marqueur de la croissance cristalline: Mise en évidence par les traces de fission dans les zircons gemmes d'Espaly (Haute-Loire, France). {Uranium as indicator of crystal growth: Evidence from fission tracks in zircon crystals from Espaly (Haute-Loire, France)}. Bull. Minéral. **110**, 459-463.

Caruba R (1979). Etude expérimentale de la cristallochimie, de la morphologie, de la stabilité et de la genèse du zircon et des zircono-silicates en vue d'applications pétrogénétiques. (Experimental study of crystal chemistry and morphology of zircons for petrological application). Thèse Doctorat ès Sciences, Université de Nice, France.

Caruba R, Turco G, Iacconi P, Keller P (1974). Solution solide d'éléments de transition trivalents dans le zircon et l'oxyde de zirconium. (Trivalent transition elements solid solution within the zircon and the zirconium oxide). Bull. Soc. Fr. Minéral. Cristallogr. **94**, 427-436.

Caruba R, Mano J, Dars R, Turco G (1975). Corrosions expérimentales de cristaux de zircons et comparison avec des corrosions naturelles de zircons de granites albitisés. (Experimental corrosion of zircon crystals, and comparison with natural corrosion of zircon from albitized granites). Tschermaks Min. Petr. Mitt. **21**, 33-46.

Caruba R, Baumer A, Gantaume M, Iacconi P (1985). An experimental study of hydroxyl groups and water in synthetic and natural zircons: a model of the metamict state. Amer. Mineral. **70**, 1224-1231.

Caruba R, Baumer A., Hartman P (1988). Crystal growth of synthetic zircon round natural seeds. J. Crystal Growth **88**, 297-302.

Cesbron F, Lulin JM, Parfenoff A (1985). Un type de zircon exceptionnel: Le zircon tabulaire {001} du complexe alcalin de Meponda (Mozambique); signification génétique. (An exceptional type of zircon: The {001} tabular zircon from Meponda alkaline complex (Mozambique); genetic signification). Bull. Minéral. **108**, 825-828.

Cesbron F, Ohnenstetter D, Blanc P, Rouer O, Sichère MC (1993). Incorporation de terres rares dans des zircons de synthèse: Etude par cathodoluminescence. (Incorporation of rare-earth elements in synthetic zircons: A cathodoluminescence study). C.R. Acad. Sci. Paris, série II, **316**, 1231-1238.

Chakoumakos BC, Muramaki T, Lumpkin GR, Ewing C (1987). Alpha-decay-induced fracturing in zircon: The transition from the crystalline to the metamict state. Science **236**, 1556-1559.

Chrustschoff K von (1892). Ueber kunstliche Darstellung des Zircons auf Nassen-Wege (On the synthetic reproduction of zircon by hydrothermal process). Jb. Mineral. **2**, 232-236.

Correia Neves JM, Lopez Nunes JE, Sahama TG (1974). High hafnium members of the zircon-hafnon series from the pegmatites of Zambézia, Mozambique. Contrib. Mineral. Petrol. **48**, 73-80.

Coy-Yll R (1969/70). Quelques aspects de la cathodoluminescence des minéraux. (Some aspects of cathodoluminescence of minerals). Chem. Geol. **5**, 243-254.

Dennen WH, Shields R (1956). Yttria in zircon. Amer. Mineral. **41**, 655-656.

Dharmarajan R, Belt RF, Puttbach RC (1972). Hydrothermal and flux growth of zircon crystals. J. Crystal Growth **13/14**, 535-539.

Eskova EM (1959). Geochemistry of Nb and Ta in the nepheline syenite massifs of the Vishnevyie Mountain. Geochem. **3**, 158-170.

Fielding PE (1970). Colour centers in zircon containing both Eu^{3+} and U^{4+} ions. Aust. J. Chem. **23**, 1513-1521

Frondel C (1953). Hydroxyl substitution in thorite and zircon. Amer. Mineral. **38**, 1007-1018.

Frondel C, Colette RL (1957). Hydrothermal synthesis of zircon, thorite and huttonite. Amer. Mineral. **42**, 759-765.

Hanchar JM, Marshall DJ (1995). Multi-laboratory results for the cathodoluminescence emission spectrum from a synthetic zircon standard. Scanning Microscopy Suppl. **9** (this volume),

Hanchar JM, Miller CF (1993). Zircon zonation patterns as revealed by cathodoluminescence and backscattered electron images: Implications for interpretation of complex crustal histories. Chem. Geol. **110**, 1-13.

Hautefeuille P, Perrey A (1898). Sur la reproduction du zircon. (About the reproduction of zircon). C.R. Acad. Sci. Paris, **107**, 1000-1001.

Hazen RM, Finger LW (1979). Crystal structure and compressibility of zircon at high pressure. Amer. Mineral. **64**, 196-201.

Henry DJ, Toney JB (1987). Combined cathodoluminescence: Backscattered electron imaging and trace element analysis with the electron microprobe: Application to geological materials. In: Microbeam Analysis. San Francisco Press, CA. pp. 339-342

Iacconi P (1995). Thermoluminescence of zircon. Scanning Microsc. Suppl. **9**, 13-34 (this volume).

Iacconi P, Caruba R (1977). Sur le role des OH^- dans l'émission de thermoluminescence du zircon $Zr(SiO_4)_{1-x}$ $(OH)_{4x}$ synthétique. (Role of OH^- on the thermoluminescence properties of zircons). CR. Acad. Sc. Paris **285**, 227-229.

Iacconi P, Caruba R (1980). Trapping and emission centers in X-irradiated natural zircon. III. Influence of trivalent rare earth impurities. phys. stat. sol. (a) **62**, 589-596.

Iacconi P, Caruba R (1984). Trapping and emission centers in X-irradiated natural zircon. Characterization by thermoluminescence. Phys. Chem. Mineral. **11**, 195-203.

Jain VK (1978). Thermoluminescence glow curves and spectrum of zircon (sand). Bull. Minéral. **101**, 358-362.

Kirsh Y, Townsend PD (1987). Electron and hole centers produced in zircon by X-irradiation at room temperature. J. Phys. C: Solid St. Phys. **20**, 967-980.

Long JVO, Agrell O (1965). The cathodo-luminescence of minerals in thin section. Mineral. Mag. **34**, 318-326.

Marfunin AS (1979) Spectroscopy, Luminescence and Radiation Centers in Minerals. Marfunin AS (ed.). Springer Verlag, Berlin. pp. 196-211.

Mariano AN (1988). Some further geological applications of cathodoluminescence. In: Cathodoluminescence of Geological Materials. Marshall DJ (ed.). Unwin Hyman, London. pp. 94-123.

Mariano AN (1989). Cathodoluminescence emission spectra of rare earth activators in minerals. In: Geochemistry and Mineralogy of Rare Earth Elements. Lipin BR, Mckay GA (eds). Reviews in Mineralogy, vol. 21. Mineralogical Society of America, Washington, DC. pp. 339-348.

Marshall DJ (1988). Cathodoluminescence of Geological Materials. Unwin Hyman, London. pp. 55-56.

Medenbach O (1976). Geochemie der elemente in Zirkon und ihre räumlische Verteilung. Eine Untersuchung mit der Electronenstrahlmikrosonde. (Geochemistry of elements in zircon and their spatial distribution. a study with the electronmicroprobe). Diplom Arbeit (thesis), Ruprecht Karl Universität, Heidelberg, Germany.

Monod-Herzen G (1966) Luminescence; l'Electron et la Lumière, Matière et Photoluminescence. (Luminescence: Electron and Light, Solid and photoluminescence). Dunod, Paris. pp. 244-246.

Ohnenstetter D, Cesbron F, Rémond G, Caruba R, Claude JM (1991). Emissions de cathodoluminescence de deux populations de zircons naturels: Tentative d'interprétation.(Tentative interpretation of cathodoluminescence emissions displayed by the two populations of natural zircons). C.R. Acad. Sci. Paris **313**, série II, 641-647.

Pellas P (1954). Sur la formation de l'état métamicte dans le zircon. (On the formation of metamict state in zircon). Bull. Soc. Fr. Min. Cristallogr. **77**, 447-460.

Pupin JP (1976). Signification des caractères morphologiques du zircon commun des roches en pétrologie. Base de la méthode typologique. Applications. (Significance of the morphologic characteristics of zircon common in rocks in petrology. Basis of the method. Applications). Thèse ès Sciences, University of Nice.

Pupin JP (1980). Zircon and granite petrology. Contrib. Mineral. Petrol. **73**, 207-220.

Pupin JP (1992). Les zircons des granites océaniques et continentaux: Couplage typologie-géochimie des éléments en traces. (Zircon from oceanic and continental granites: Coupled study typology-trace element geochemistry). Bull. Soc. Géol. Fr. **163**, 495-507.

Pupin JP, Turco G (1972). Une typologie originale du zircon accessoire. (An original typology for accessory zircon). Bull. Soc. Fr. Minéral. Cristallogr. **95**, 348-359.

Pupin JP, Turco G (1975). Typologie du zircon accessoire dans les roches plutoniques dioritiques, granitiques et syénitiques. Facteurs essentiels déterminant les variations typologiques. (Typology of accessory zircon in dioritic, granitic and syenitic plutonic rocks. Essential parameters controlling the typologic variations). Pétrologie **1**, 139-156.

Rémond G, Kimoto S, Okuzumi H (1970). Use of the SEM in cathodoluminescence observation in natural specimens. Scanning Electron Microsc. **1970**, 33-40.

Rémond G (1977). Applications of cathodoluminescence in mineralogy. J. Lumin. **15**, 121-155.

Rémond G, Cesbron F, Chapoulie R, Ohnenstetter D, Roques-Carmes C, Schvoerer M (1992). Cathodoluminescence applied to the microcharacterization of min-

eral materials: A present status in experimentation and interpretation. Scanning Microsc. **6**, 23-68.

Rémond G, Gilles C, Isabelle D, Choi C, Azahra M, Rouer O, Cesbron F (1995a). Electron and proton induced X-ray spectrometry: Two complementary spatially resolved analytical techniques in mineralogy. Appl. Radiat. Isot. **46**, 563-570.

Rémond G, Blanc P, Cesbron F, Ohnenstetter D, Rouer O (1995b). Cathodoluminescence of rare earth doped zircons II: Relationship between the distribution of the doping elements and the contrasts of images. Scanning Microsc. Suppl. **9**, 57-78.

Robinson GW (1979). The occurrence of rare earth elements in zircon. Ph.D. Thesis, Queen's University, Kingston, Ontario, Canada.

Robinson K, Gibbs GV, Ribbe PH (1971). The structure of zircon: A comparison with garnet. Amer. Mineral. **56**, 782-790.

Sainte-Claire Deville H, Caron H (1858). Sur un nouveau mode de production à l'état cristallisé d'un certain nombre d'espèces chimiques et minéralogiques. (New method of synthesis of crystals of various substances). C. R. Acad. Sci. Paris **46**, 764-768.

Smith DGW, St. Jorre L de, Reed SJB, Long JVP (1991). Zonally metamictized and other zircons from Thor lake, Northwest Territories. Can. Mineral. **29**, 301-309.

Smith JV, Stenstrom RC (1965). Electron-excited luminescence as a petrologic tool. J. Geol. **73**, 627-655.

Soltnsev VP, Shcherbakova MY (1974). Charge compensation mechanisms and the form in which Nb and Y are incorporated into the structure of zircon. Neorg. Mat. **10/10**, 1834-1838.

Speer JA (1982). Zircon. In: Orthosilicates. 2nd ed. Reviews in Mineralogy, Vol. **5**. Ribbe PH (ed). Mineralogical Society of America, Washington, DC. pp. 67-112.

Uhrin R, Belt RF, Puttbach RC (1974). The hydrothermal growth of zircon. J. Crystal Growth **21**, 45-68.

Vinokurov VM, Gainullina NM, Evgrafova LA, Nizamutdinov NM, Suslina AN (1971). Zr^{4+}-Y^{3+} isomorphism in zircon and the associated charge compensation. Soviet Physics Crystallography **16**, 262-265.

Votyakov SL, Krokhalev VYa, Krasnobaev AA (1985). Zircon recombination luminescence. J. Appl. Spectrosc. **42**, 633-638.

Votyakov SL, Ivanov IP, Krasnobaev AA, Krokhalev VYa, Korzhinskaya VS (1986). Luminescence-spectral properties of zirconium orthosilicate prepared by hydrothermal method. Inorg. Mater. **22**, 239-244.

Yang B, Luff BJ, Townsend PD (1992). Cathodoluminescence of naturals zircons. J. Phys. Matter **4**, 5617-5624.

Yang C, Homman NP-O, Malmqvist KG, Johansson L, Halden NM, Barbin V (1995). Ionoluminescence: A new tool for nuclear microprobes in geology. Scanning Microsc. **9**, 43-62.

Discussion with Reviewers

D.J. Marshall: Figures 8, 9 and 10 show the variations in the spectrum with electron beam energy and electron beam current (intensity). How reproducible are these results? Are they the same if the data are taken in arbitrary order, e.g., 3, 12, 10, 5, and 7 kV versus 3, 5, 7, 10, and 12; or if the first curve is repeated after the others are taken, e.g., 3, 5, 7, 10, 12, and 3 kV?

Authors: This question relates to the general problem of electrostatic charging of insulators and its consequence on the reliability of quantitative data derived from all signals induced by the incident electron beam.

The CL intensity measured at the surface of an insulator as a function of the excitation conditions can be summarized by the following expression:

$$I_{CL} = f(i_b, d, t)\,(V - V_0)^q$$

where, i_b is the incident electron beam current, d the beam diameter, t the acquisition time, V the accelerating voltage and V_0 the "dead voltage". The CL intensity depends on an excitation threshold V_0 indicating that the radiative charge recombination mechanisms is a function of the depth below the specimen surface. By increasing the accelerating voltage (i.e., by increasing the electron penetration depth), the changes in the relative intensities of the intrinsic CL may indicate a variation in the density of defects (created during the crystal growth) at different depths. After a measurement performed with a particular incident energy value, an electric charge will remain trapped within the bulk material. The depth of the trapped charge will depend of the incident energy used. When experiments are repeated by varying the incident energy, the initial trapped charges will differently modify the ionization depth distributions.

We have previously investigated the effects of charging in X-ray spectrometry using soft emission bands; those results can be reasonably extended to CL emission because the microscopic causes responsible for electrostatic charging (electron traps within the bandgap of the crystal) are the same as those involved in the luminescence process.

The charge conservation law at the electron beam spot at the specimen surface leads to:

$$I_b = (\delta + \eta)\, I_b + I_s + dQ/dt$$

where, I_b is the incident beam current, I_s the specimen current, δ and η the secondary and backscattered electron coefficients, respectively, and dQ/dt is the trapped charge per unit time. For a conductive material, dQ/dt = 0. For insulating materials, part of the incident electrons remain trapped and dQ/qt is not zero except when a steady stated is reached. For the steady state, dQ/dt is equal to zero, but the steady charge Q is not equal to zero and an electric field is established inside the insulator. While examining a specimen coated with a metallic film, the surface potential is zero and no beam displacement can occur. However, while the surface coating prevents against surface charging, the charge trapping inside the bulk of the sample still occurs and the created electric field may be very strong and can reduce the depth of penetration of the incident electrons. These internal fields increase the electron backscatter coefficient leading to an increase of the ionization function at the specimen surface as compared to that for a conductive material. These effects will modify the shape and the intensities on the CL emission spectra, when measured following a high energy pre-irradiation. Experimental verification of this explanation is still needed.

D.J. Marshall: Can you say a little more about why the spectra are affected by the intensity of the beam?

J.M. Hanchar: Is it not possible that the different ways in which the zircons were grown could lead to different numbers of defects thus leading to variations in the intrinsic CL emission as pointed out by Votyakov (1985). I do not think that the variations in the intrinsic CL are due to electron bombardment. I think it would be very difficult to tell whether trace element impurities versus defects related to the synthesis technique are responsible for the UV CL variations.

Authors: As discussed above, a charge will remain trapped at a depth below the specimen surface depending on the incident energy. The charge will also depend on the incident dose. The intensities of the emitted signals will vary when the diameter of incident beam is varied or when a rastered beam is used instead of a stationary beam. The development of strong internal electric fields not only modify the energy loss distribution but will also induce migration of mobile ions. Such ion migration driven by the internal electrical field modifies the surface composition. Beam damage during electron bombardment of silicates result in the formation of oxygen bubbles which escape from the specimen into the vacuum [Lineweaver JL (1963) Oxygen outgassing by electron bombardment of glass, J. Appl. Phys. **34**, 1786-1791]. The electron irradiation will modify the filling of the existing electron traps and/or create new structural defects, modifying subsequently the intrinsic CL emission bands.

J.M. Hanchar: How can the authors rule that some of the CL peaks they measured in their REE doped synthetic zircons are due to REE impurities in the starting materials (either the ZrO_2, or the REE oxides and carbonates)? I too used spectroscopic grade oxides in my synthetic zircon work and I detected Dy^{3+} CL emission lines in my undoped as well as in my La, Ce, Nd, Ho, Tm, Yb, and Lu doped zircons. The Dy^{3+} peaks were very small, but none the less were present in these zircons. In other words, have the authors correlated the major CL peaks for each REE doped zircon with known 4f electronic transitions?

Authors: According to the analytical certificate from Johnson Matthey, the Specpure grade REE oxides used contain no more than a few tenths ppm of the other REE oxides. These small amounts of REE may be sufficient to produce very weak CL characteristic peaks. However the intensities of these unwanted lines will be low and will no affect significantly the shape and the intensities of the CL emission spectrum of the major doping REE.